SANDIA REPORT
SAND2015-6694
Unlimited Release
July 2015

Can symmetry transitions of complex fields enable 3-d control of fluid vorticity?

James E. Martin and Kyle J. Solis

Prepared by
Sandia National Laboratories
Albuquerque, New Mexico 87185 and Livermore, California 94550

Sandia National Laboratories is a multi-program laboratory managed and operated by Sandia Corporation, a wholly owned subsidiary of Lockheed Martin Corporation, for the U.S. Department of Energy's National Nuclear Security Administration under contract DE-AC04-94AL85000.

Approved for public release; further dissemination unlimited.

Sandia National Laboratories

Issued by Sandia National Laboratories, operated for the United States Department of Energy by Sandia Corporation.

NOTICE: This report was prepared as an account of work sponsored by an agency of the United States Government. Neither the United States Government, nor any agency thereof, nor any of their employees, nor any of their contractors, subcontractors, or their employees, make any warranty, express or implied, or assume any legal liability or responsibility for the accuracy, completeness, or usefulness of any information, apparatus, product, or process disclosed, or represent that its use would not infringe privately owned rights. Reference herein to any specific commercial product, process, or service by trade name, trademark, manufacturer, or otherwise, does not necessarily constitute or imply its endorsement, recommendation, or favoring by the United States Government, any agency thereof, or any of their contractors or subcontractors. The views and opinions expressed herein do not necessarily state or reflect those of the United States Government, any agency thereof, or any of their contractors.

Printed in the United States of America. This report has been reproduced directly from the best available copy.

Available to DOE and DOE contractors from
U.S. Department of Energy
Office of Scientific and Technical Information
P.O. Box 62
Oak Ridge, TN 37831

Telephone: (865) 576-8401
Facsimile: (865) 576-5728
E-Mail: reports@osti.gov
Online ordering: http://www.osti.gov/scitech

Available to the public from
U.S. Department of Commerce
National Technical Information Service
5301 Shawnee Rd
Alexandria, VA 22312

Telephone: (800) 553-6847
Facsimile: (703) 605-6900
E-Mail: orders@ntis.gov
Online order: http://www.ntis.gov/search

SAND2015-6694
Unlimited Release
July 2015

Can symmetry transitions of complex fields enable 3-d control of fluid vorticity?

James E. Martin and Kyle J. Solis
Org. 1124, Nano-Sciences Department
Sandia National Laboratories
P.O. Box 5800, MS 1415
Albuquerque, New Mexico 87185-1415

Abstract

Methods of inducing vigorous noncontact fluid flow are important to technologies involving heat and mass transfer and fluid mixing, since they eliminate the need for moving parts, pipes and seals, all of which compromise system reliability. Unfortunately, traditional noncontact flow methods are few, and have limitations of their own. We have discovered two classes of fields that can induce fluid vorticity without requiring either gravity or a thermal gradient. The first class we call Symmetry-Breaking Rational Fields. These are triaxial fields comprised of three orthogonal components, two ac and one dc. The second class is Rational Triad Fields, which differ in that all three components are alternating. In this report we quantify the induced vorticity for a wide variety of fields and consider symmetry transitions between these field types. These transitions give rise to orbiting vorticity vectors, a technology for non-contact, non-stationary fluid mixing.

ACKNOWLEDGMENTS

Sandia National Laboratories is a multi-program laboratory managed and operated by Sandia Corporation, a wholly owned subsidiary of Lockheed Martin Corporation, for the U.S. Department of Energy's National Nuclear Security Administration under contract DE-AC04-94AL85000. This work was supported by the Division of Materials Science, Office of Basic Energy Sciences, U.S. Department of Energy (DOE). We thank Matt Groo at Novamet for supplying the magnetic platelets. We thank Jerry Simmons for supporting this work from the Fellow fund.

CONTENTS

Quantifying vorticity in magnetic particle suspensions driven by symmetric and asymmetric multiaxial fields....9

1. Introduction....9
   1.1. Symmetry Theory Background....9
   1.2. Torque Density Functional....10

2. EXPERIMENTAL....13

3. RESULTS AND DISCUSSION....15
   3.1. Computations for Symmetry-Breaking Fields....15
   3.2. Dependence on Phase and DC Field....17
   3.3. Heterodyning....18
   3.4. Torque Density for Fields of Increasing Complexity....18
   3.5. Flow Reversal....21
   3.6. Inducing Vorticity with Biaxial Fields?....22
   3.7. Rational Triads....23

4. Summary....29

Creating orbiting vorticity vectors in magnetic particle suspensions through field symmetry transitions — a route to multi-axis mixing....31

5. Introduction To vorticity Orbits....31

6. Field Symmetry Transitions....33
   6.1. Even, Odd, Odd Fields....34
   6.2. Odd, Even, Even Fields where Even:Even Factors to Odd:Even....35
   6.3. Odd, Even, Even Fields where Even:Even Factors to Odd:Odd....36
   6.4. Odd:Odd:Odd Fields....36
   6.5. Torque density functional....36
   6.6 Predicted torque densities along the three field components....38
   6.7 The prediction of vorticity orbits....43
   6.8 Experimental set up....45
   6.9 Results and Discussion....46

7. Conclusions....53

8. References....55

9. Distribution....57

FIGURES

Figure 1. Instantaneous values of the computed torque functional....16
Figure 2. Computed torque density as a function of the high frequency phase for the 2:3:dc field....17
Figure 3. When a 2:3:dc field is detuned field to 101:150:dc....18
Figure 4. The maximum of the torque functional as a function of phase....19
Figure 5. The maximum of the torque functional as a function of phase....20
Figure 6. The Fibonacci sequence creates a periodic transition....21
Figure 7. For all of the odd:odd+1:dc fields we have investigated (1:2, 3:4,…)....21
Figure 8. When a dc field is applied along the high frequency axis of a 2:3 field....22

Figure 9. The torque functional correctly predicts torque 24
Figure 10. The torque functional correctly predicts torque around the *x* axis 26
Figure 11. The torque functional predicts torque around all axes 27
Figure 12. The torque functional predicts torque around all axes for the 1:3:5 field: 28
Figure 13. The field symmetry transition is illustrated for the 1+dc:2:3 triaxial field. 35
Figure 14. Torque components along all three axes for a 1+dc:2:3 field with a *c*=0.5. 37
Figure 15. The nature of the continuous vorticity transition 39
Figure 16. The data in Fig. 15 are presented, ...40
Figure 17. The torque component along y for a 1:2:3 field 41
Figure 18. Transects 42
Figure 19. The heterodyne orbits 44
Figure 20. Complex vorticity vector orbits 45
Figure 21. Experimental torque density plots 47
Figure 22. (top) The locus of possible vorticity vectors 48
Figure 23. Experimental vorticity orbits along the four transects 50
Figure 24. Phase offsets significantly alter the vorticity orbits 51
Figure 25. For the phase modulated 1+dc:2:3 with *c*=0.7, ...52

NOMENCLATURE

DOE	Department of Energy
SNL	Sandia National Laboratories

QUANTIFYING VORTICITY IN MAGNETIC PARTICLE SUSPENSIONS DRIVEN BY SYMMETRIC AND ASYMMETRIC MULTIAXIAL FIELDS

1. INTRODUCTION

Methods of inducing vigorous noncontact fluid flow are important to technologies involving heat and mass transfer and fluid mixing, since they eliminate the need for moving parts, pipes and seals, all of which compromise reliability. Unfortunately, noncontact methods of inducing strong organized flows are few, and have limitations of their own. For example, natural convection [1–3] requires both gravity and a destabilizing thermal gradient. Magnetohydrodynamics [1] requires the injection of large currents into conducting liquids and high magnetic fields. Thermomagnetic convection in ferrofluids [4,5] requires gravity, a destabilizing thermal gradient and a large magnetic field gradient, which makes scaling to large volumes challenging. A more flexible method that eliminated these requirements would be amenable to a broad range of applications.

We have discovered several classes of triaxial fields of modest strength that induce vigorous noncontact fluid flow in dilute magnetic particle dispersions without requiring gravity, a thermal gradient, or a magnetic field gradient. Such fields can create flow lattices [6], vortex lattices and vortex fluids [7, 8]. These induced flows have been used to direct droplet motion [9], create a thermal valve [10], effect active, directed wetting [7], and stimulate a variety of biomimetic dynamics [9]. However, at this point our understanding of these flows is based only on the symmetry of the multiaxial fields and this non-quantitative approach is useful only for certain highly symmetric fields. In this study a functional of the magnetic field is introduced that pertains to the measurable fluid torque densities. The purpose of this study is to investigate the degree to which this functional conforms to the wide range of observed phenomena, to demonstrate that it conforms to the many predictions of symmetry theory, and to use this functional to make predictions where symmetry theory cannot be applied.

1.1. Symmetry Theory Background

The symmetry theories we have developed are for two classes of fields that induce vorticity, each of which is comprised of three orthogonal components. The first class we call *symmetry-breaking rational fields* [7,8]. These fields employ two alternating components and one dc component. The frequencies of the ac components form a rational number l:m, where l and m are relative primes, so either one or both are odd. The second class of fields we call *rational triads* [11], which differ in that all three components are alternating. Once again the frequency ratios are rational numbers, such as 1:2:3. For both field classes it can be shown that the dynamic fields have the symmetry of vorticity and thus have the parity required to allow deterministic fluid vorticity and flow reversal.

The primary goal of the symmetry theories is to predict whether deterministic vorticity can occur and if so, to predict the direction of the fluid vorticity vector and the field changes required to reverse the sign of the vorticity without changing its magnitude. For symmetry-breaking rational fields the predictions are that the vorticity axis is parallel to the odd axis unless both axes are odd, in which case it is parallel to the dc field. Only if the vorticity is around an ac axis does reversing the dc field reverse the flow, but changing the phase of the high frequency (m) component by $180°/l$ ($l \leq m$) always reverses the flow. These predictions have been experimentally confirmed for all fields investigated [8].

For rational triads the symmetry theory predicts that vorticity occurs around the field component whose reduced frequency has unique numerical parity (*e.g.*, the "2" in 1:2:3). In the case where all reduced frequencies are odd (*e.g.*, 1:3:5) the dynamic field does not have the symmetry of vorticity, so it is not possible to make predictions about flow with this approach. Symmetry theory also predicts the phase changes required to reverse flow at constant magnitude. These predictions have also been confirmed for the fields we have investigated [11].

Symmetry theory has some limitations. First, it is not possible to make predictions for fields whose Lissajous trajectories are not highly symmetrical. For symmetry-breaking fields these 2-d trajectories occur at particular phase angles between the two ac components. For example, for a 1:2 field these special phase angles (applied to the high frequency component) are 0°, 90°, 180°,... In all cases there are four distinct Lissajous trajectories that can be treated out of this 1-d set of continuous phases. All other phase angles cannot be treated. For rational triads the symmetric Lissajous trajectories can be obtained by applying the phase angles 0°, 90°, 180°,… to each of the three frequencies in any combination. It turns out that this creates only 16 distinct 3-d Lissajous trajectories that can be analyzed out of the 2-d set of independent phase angles (there are only two independent phases for three frequencies since the zero of time is unimportant).

A second limitation of symmetry theory is the inability to make any kind of estimate of the *magnitude* of the torque density created within a magnetic particle dispersion subjected to a multiaxial field. Intuitively, it is reasonable that a 1:2 symmetry-breaking field will create greater vorticity than a 13:20 field, but there is currently no method of justifying this belief. Even more disconcerting is the inability to deal with the effect of small frequency changes. For example, the symmetry-breaking field 150:100 factors to 3:2, so vorticity is predicted to occur around the high-frequency field axis. But if the low frequency is increased to obtain 150:101 the low frequency axis becomes odd so vorticity should now occur around this axis. But 150:101 can be viewed as a phase-modulated 3:2 field, so we expect to observe oscillating vorticity around the high frequency axis, which is indeed the experimental observation. Symmetry theory cannot address this oscillating flow.

Finally, symmetry theory cannot address the utter peculiarity of the origin of these flows. There is just something strange about predicting vorticity for fields that in general are non-circulating. Yet these flows can be quite vigorous. In fact, the symmetry theory only shows that these flows are allowed and cannot make any statement about whether they should or should not occur. For these reasons it is desirable to have a physically reasonable method that for any given field can produce a torque density vector that produces vorticity. One approach is to simulate the system microscopically. This would lead to an understanding of the microscopic magnetic particle dynamics as well as addressing the issues raised above, but such an approach would be extremely time-consuming. A second approach is to develop a closed-form theory of the microscopic particle dynamics that can at least be numerically integrated. A third approach is to use physical insight and previous results to develop a functional that produces the torque vector: This is the approach we have taken as a first step on the path to quantifying vorticity in any multiaxial field.

1.2. Torque Density Functional

A physically meaningful functional must conform to all of the above-mentioned predictions of the symmetry theories and yet must also conform to various experimental observations. These observations include the finding that the torque density in a particle suspension exposed to a particular field is independent of particle size, liquid viscosity, and the magnitude of the field frequencies, provided that the *Mason* number is below a critical value that permits particle chaining. For the restricted case of a "vortex field," which consists of a rotating field to which an orthogonal dc field is applied, an expression has been derived for the suspension torque density

that is based on the analysis of *volatile* particle chains that lag in phase behind the field [12]. This is a phase lag problem in three dimensions for particle chains whose size is determined by various instabilities that lead to fragmentation. This theory successfully accounts for all of the experimental observations on vortex fields, the result being

$$\mathrm{T} = \frac{1}{12}\varphi_p \mu_0 M^2 \sqrt{\sin^2\theta_f - \cos^2\theta_f} \text{ for } \theta_f \geq 45° \tag{1}$$

where φ_p is the particle volume fraction, μ_0 is the vacuum permeability, M is the particle magnetization, and θ_f is the angle the field vector makes to the dc field. For this case the Mason number is defined as $Mn = 9\eta\omega/(2\mu_0 M^2)$, where □ is the field frequency. Eq. 1 is valid when this Mason number is less than ~0.02 for *balanced* vortex fields, those having equal rms field components ($\tan\theta_f = \sqrt{2}$). In the case of linear magnetic polarization the particle magnetization for a dilute suspension is given by $\chi_p H_0$ where $\chi_p = 3$ is the intrinsic susceptibility of a magnetic sphere comprised of a material whose relative permeability greatly exceeds that of the liquid, which is the typical case for soft ferromagnetic particles. In short, the specific torque density T/φ_p is simply proportional to the energy density $\mu_0 H_0^2$ of the field.

The vortex field is a very simple case because it admits a steady-state solution. For other multiaxial fields, such as 1:2:dc the field magnitude is not constant and the axis about which instantaneous field rotation occurs is not so easily described. If we make the approximation that the instantaneous field energy density gives the instantaneous torque density then all that remains is dealing with the direction of the instantaneous torque vector. As a second approximation this torque direction is taken to be the direction about which the instantaneous field rotates, $\mathbf{H}_0(t)\times\dot{\mathbf{H}}_0(t)/\left|\mathbf{H}_0(t)\times\dot{\mathbf{H}}_0(t)\right|$, in other words this vector is normal to the instantaneous rotation plane of the field. If the torque is indeed caused by particle chains lagging the field, then this is a good approximation when the phase lag is small. The torque density functional **M** is thus

$$\mathbf{M} = \int_0^1 \mathbf{M}(s)\,ds \text{ where } \mathbf{M}(s) = \left|\mathbf{h}(s)\right|^2 \frac{\mathbf{h}(s)\times\dot{\mathbf{h}}(s)}{\left|\mathbf{h}(s)\times\dot{\mathbf{h}}(s)\right|}. \tag{2}$$

Here $s = ft$ is the reduced time, f is a frequency, and **h** is the reduced field. For symmetry breaking fields the reduced field is

$$\mathbf{h}(t) = \frac{\mathbf{H}_0(t)}{H_0} = \sin(l\times 2\pi ft + \phi_l)\hat{\mathbf{x}} + \sin(m\times 2\pi ft + \phi_m)\hat{\mathbf{y}} + \frac{c}{\sqrt{2}}\hat{\mathbf{z}} \tag{3}$$

l and m are relative primes and by convention $l \leq m$. The rms reduced field is $\sqrt{2+c^2}/\sqrt{2}$. (For a balanced field, where all rms field components are equal $c = 1$.) For the rational triads we restrict our attention to such balanced fields, so

$$\mathbf{h}(t) = \sin(l\times 2\pi ft + \phi_l)\hat{\mathbf{x}} + \sin(m\times 2\pi ft + \phi_m)\hat{\mathbf{y}} + \sin(n\times 2\pi ft + \phi_n)\hat{\mathbf{z}} \tag{4}$$

In this case the rms reduced field is $\sqrt{3/2}$ and to be definite $l \leq m \leq n$. The predicted torque density is related to the dimensionless torque density functional by $\mathbf{T} = const\times\varphi_p\mu_0 H_0^2\mathbf{M}$.

This expression may be viewed as an *ansatz*, not a theory *per se,* however it produces many useful results that are in accord with experiment and also can be used to successfully

predict unexpected effects that we have observed in experiment. Some of these predictions were sufficiently strange that we literally ran down to the lab to verify them, and verify them we did, as will be discussed below.

2. EXPERIMENTAL

The magnetic particle suspension consisted of molybdenum-Permalloy platelets ~50 m across by 0.4 m thick (Novamet Corp.) dispersed into isopropyl alcohol at a low volume fraction. The uniform triaxial ac magnetic fields were produced by three orthogonally-nested Helmholtz coils, operating in series resonance with appropriately-configured capacitor banks, two of which employ a computer-controlled fractal design [13]. For the 1:3:5 rational triad field studied in this work the fundamental frequency was 50 Hz and all three induction field components were 150 Grms. The three field components were phase-locked *via* two Agilent/HP function generators (equipped with Option 005), allowing for *stable* control of the phase angle of each component. (If the field components are not phase-locked there will be a very slow phase modulation between the components due to the finite difference in the oscillator frequency of each function generator, preventing meaningful studies of the phase angle.)

To quantify the magnitude of the vorticity, the torque density of the suspension was computed from measured angular displacements on a custom-built torsion balance. In this case the suspension (1.5 vol%) was contained in a small vial (1.8 mL) attached at the end of the torsion balance and suspended into the central cavity of the Helmholtz coils *via* a 96.0 cm-long, 0.75 mm-diameter nylon fiber with a torsion constant of ~13 $N \cdot m\ rad^{-1}$.

3. RESULTS AND DISCUSSION

3.1. Computations for Symmetry-Breaking Fields

The first issue that must be addressed is whether the functional conforms to the predictions of symmetry theory. The case of a 2:3:dc field with both phase angles set to zero is given in Fig. 1. Recall that vorticity must occur around the high frequency (y) axis in this case. In these figures the three components of the integrand of $\mathbf{M}(s)$ and its integral are given as functions of the reduced time. This integral corresponds to the rotation of a body subject to this time-dependent torque density. Along both the x and z axes the integrands are perfectly symmetric around zero, so the integral over one cycle is zero and the average slope of the integral, which is proportional to the average torque density, is thus zero. Along the y axis the integral is asymmetric, and the integral has a finite average slope and torque density. So this particular case conforms to the predictions of symmetry theory. In fact, even the predicted fluctuations in the torque can be observed experimentally as a jittery torque signal.

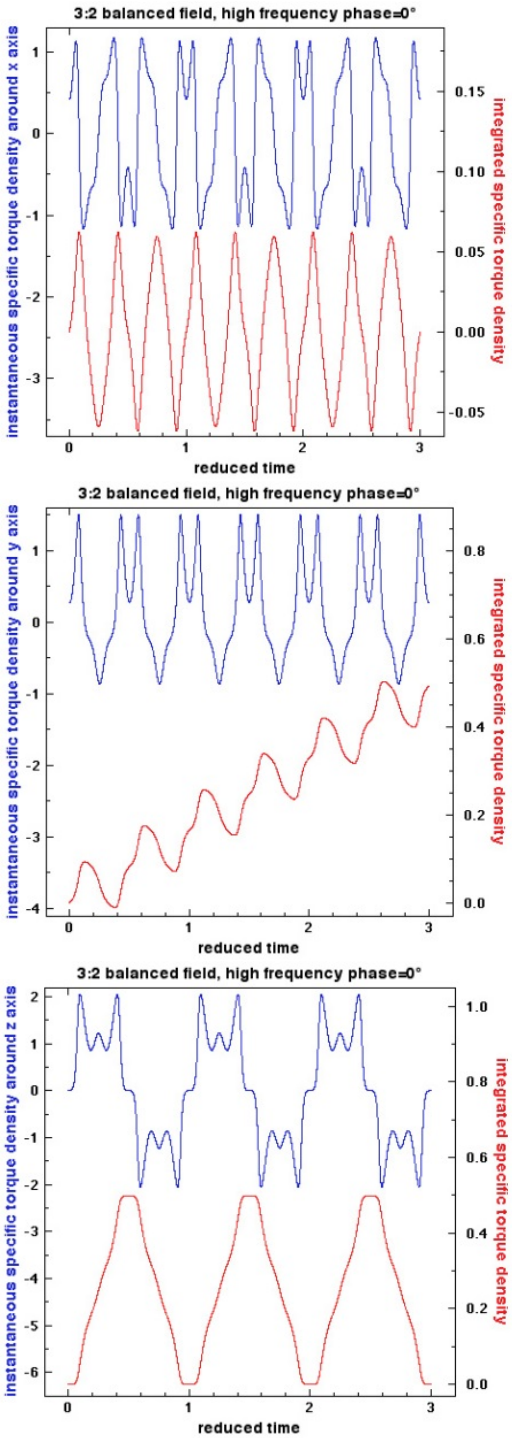

Figure 1. Instantaneous values of the computed torque functional
are given for a 2:3:dc symmetry-breaking field. The integral of these functions corresponds to the rotation of a free body subjected to this torque. A persistent rotation only occurs around the y axis, which is indeed the prediction of symmetry theory. The time-averaged torque density functional is the slope of the integral. It is this slope that pertains to measurement, since the field frequencies are typically in the audio range, generally above 48 Hz in our laboratory and frequently much higher, and so the fluctuations only give rise to rapid fluctuations of the needle in our torsion fiber apparatus.

3.2. Dependence on Phase and DC Field

The computed torque density has a strong dependence on the relative phase between the ac field components, as well as on the magnitude of the dc field. This dependence is shown in Fig. 2 for the y axis torque created by the 2:3:dc field. At zero dc field the torque functional is zero, in accordance with symmetry theory for even, odd fields, but for finite dc fields the torque is non-vanishing, is periodic on the interval 180°, and can be reversed at constant magnitude by any 90° shift of the high frequency phase, in agreement with both symmetry theory [7] and experiment [8]. Moreover, symmetry theory shows that reversing the dc field reverses the torque for even, odd fields and the torque functional also shows this reversal. In general, for the field l:m symmetry theory shows that when plotted against the high-frequency phase the torque curve is periodic on the interval 360°/l and reverses at constant magnitude for phase shifts of 180°/l.

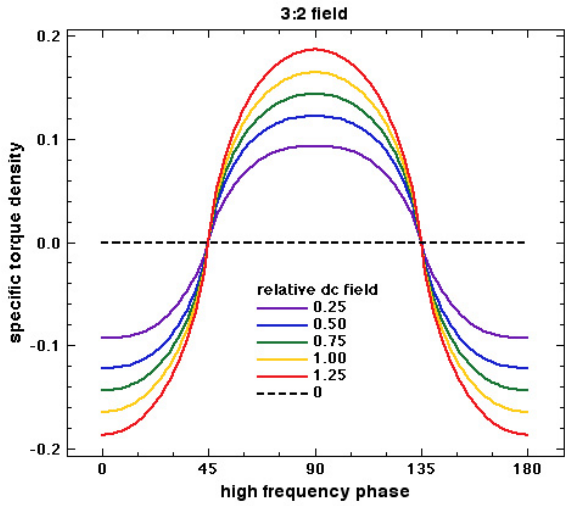

Figure 2. Computed torque density as a function of the high frequency phase for the 2:3:dc field. The dc field is relative to the rms amplitude of either of the ac field components.

Odd:odd fields differ in that vorticity is symmetry allowed even in the absence of the dc field component and therefore must not reverse upon dc field reversal. Computations for the 1:3 field do indeed show that the torque functional does not vanish in the absence of a dc field, but grows stronger as the dc field increases and cannot be reversed by reversing the dc field. This suggests the possibility of torque when the dc field is replaced by an ac field, a subject discussed below. However, the experimental situation is complicated by the fact that in the absence of the dc component the particles experience a time-averaged interaction that can be described as a negative dipolar interaction, causing the particles to form into parallel stationary sheets [14–16] (like baklava), instead of forming the volatile chains that give rise to vorticity. Because of this competing effect, fluid vorticity *does* require the presence of the dc component, at least for spherical particles. For platelets made of soft ferromagnetic materials the situation is more complex: Although stationary sheets can form in a biaxial field under some circumstances (*e.g.*, very high frequency, very high viscosity, low field), flow instabilities typically occur in the form of a square lattice of antiparallel flow columns normal to the plane of the field [6]. When these columns form in an odd:odd field there is pronounced vorticity as well, the axis of which is parallel to the flow columns. At higher platelet loadings a normal-field instability can occur that causes the particle dispersion to rise up as a ridge, within which a lattice of flow columns can be observed [see Fig. 4 in Reference 6]. The vorticity in the absence of a dc field can be easily confirmed by detuning one of the field components to create a phase modulation that periodically reverses the vorticity. The ridge then sloshes back-and-forth in response to the oscillating vorticity, which brings us to the next issue: field heterodyning.

3.3. Heterodyning

A more interesting problem is that of heterodyning, which occurs when one of the frequencies is detuned to create a modulation of phase and flow reversal. In Fig. 3 are presented computations for the case 101:150:dc. Because this is a modulation of 2:3:dc it is expected that a periodic torque around the y axis will occur, and this is indeed observed in the component $M_y(s)$. More importantly, the time-average of this torque is zero, in conformity to symmetry theory. However, symmetry theory allows a finite time-average torque around the x axis, and although this torque is quite small, the slope can be seen in the data in Fig. 3(b).

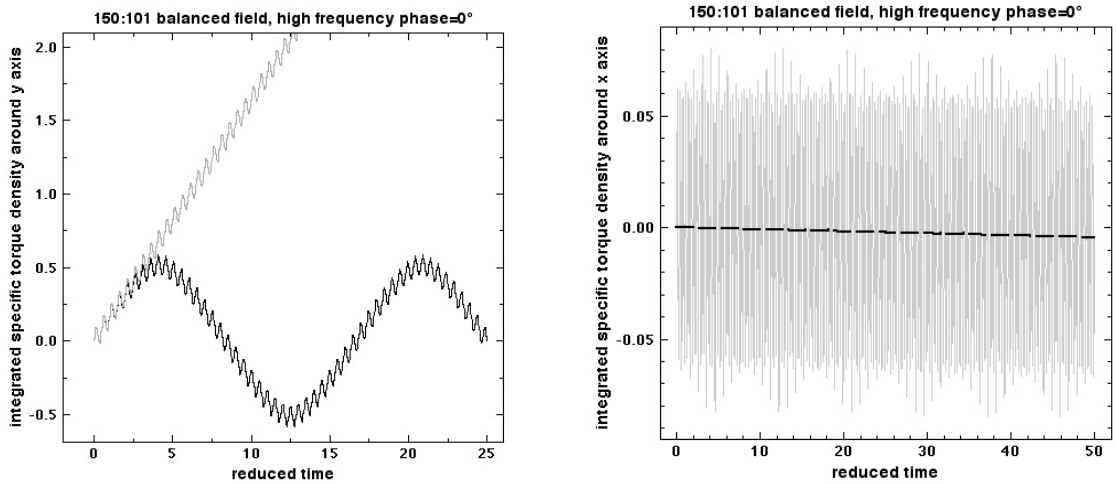

Figure 3. When a 2:3:dc field is detuned field to 101:150:dc
the heterodyne beating creates periodic flow reversal around the y axis, which is indeed observed in the laboratory. (top) The torque functional demonstrates this flow reversal and shows that the peak torque density is expected to be the same as for the non-heterodyned field. However, symmetry theory shows that for the 101:150:dc field the average torque can be non-vanishing only around the x axis. For this field the torque functional shows that around the y axis does indeed average to zero and a small but finite net torque does occur around the x axis, as shown at bottom.

3.4. Torque Density for Fields of Increasing Complexity

As the irreducible ratio of the field frequencies requires larger integers to represent, both experiment and intuition indicate that the suspension torque density diminishes, though symmetry theory is uninformative on this point. To examine this issue we have considered a few particular sequences of irreducible rational numbers. The first two sequences arise in investigations of the fractional quantum Hall effect [17] and serve as useful examples here as well. Both of these sequences approach 1/2, one from above $[k/(2k-1),\ k=1,2,\ldots]$ and one from below $[k/(2k+1),\ k=1,2,\ldots]$. All of these calculations are for balanced fields and the phase angle between the field components (either ϕ_x or ϕ_y will do) is varied to find the maximum of the torque functional.

The dependence of $|\mathbf{M}|$ on the denominator of these ratios is shown in Figs. 4(a) and 4(b). For the sequence approaching ½ from above the torque vacillates between the high frequency and dc field directions, in agreement with symmetry theory, and falls off asymptotically as the inverse of the number of domains N in the relevant Lissajous curve, given by $N = lm + (l-1)(m-1)$. Fields such as 21:41 therefore give rise to very small torques in comparison to something like 2:3. For the sequence approaching ½ from below, Fig. 4(b), the behavior is similar, with the odd:odd fields showing somewhat greater torque.

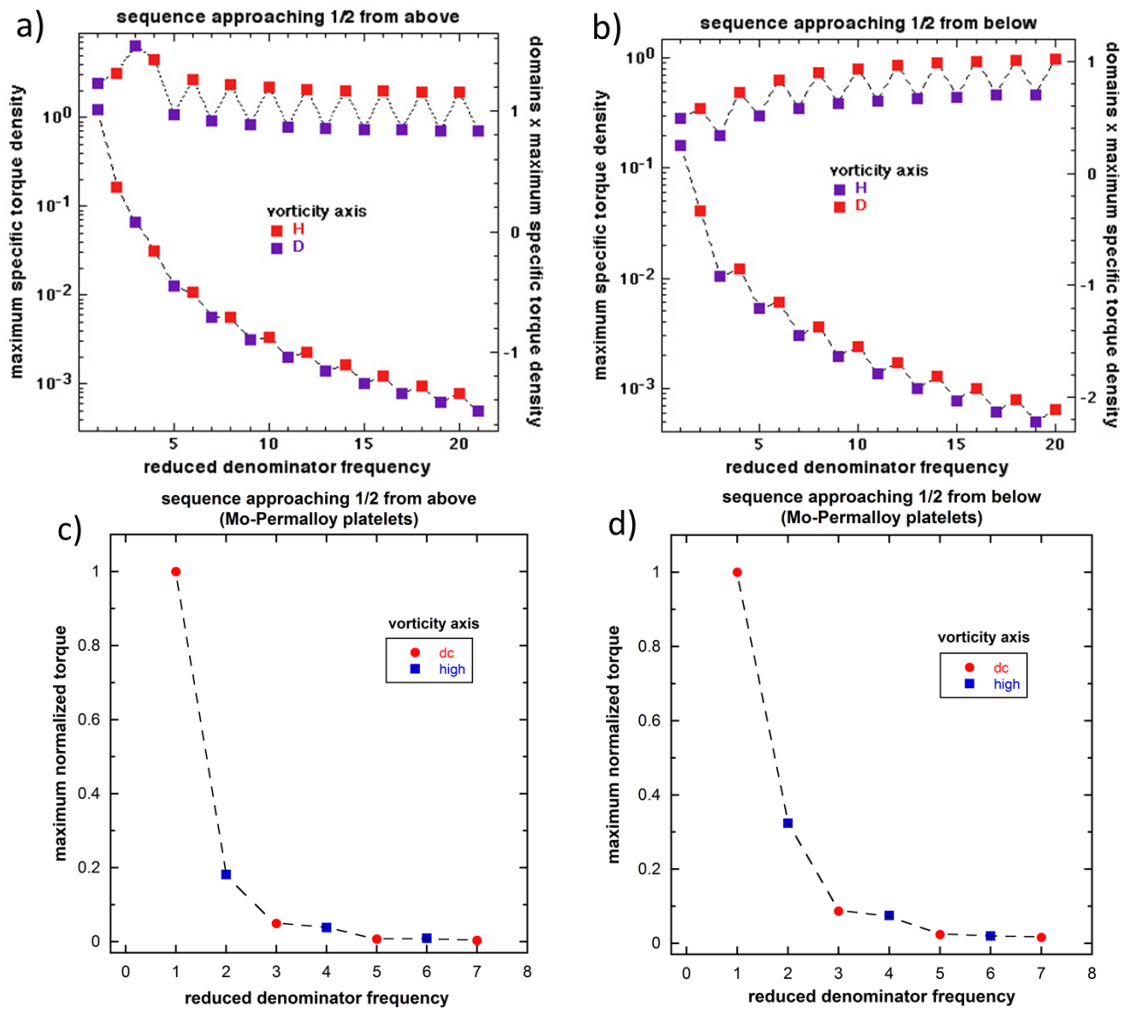

Figure 4. The maximum of the torque functional as a function of phase is plotted versus the relative denominator frequency for rational number sequences approaching ½ from above and below. Multiplying these peak torques by the number of domains in the 2-d Lissajous plots shows an approach to an asymptote, indicating an algebraic decay. The alternation in the torque axes are predicted by symmetry theory as well. (bottom) Experimental torque data for rational number sequences approaching ½ from above and below show the alternation of the vorticity axis between the high frequency and dc field axes, although the relative magnitude of the torque around each axis is reversed from the trend predicted by the functional. In both cases the magnitude of the torque is observed to decay rapidly as the number of Lissajous domains increases.

Both of these sequences were investigated experimentally, with the torque data shown in Figs. 4(c) & (d). The experimental torque values display the alternation of the vorticity axis between the high frequency and dc field axes, in accord with the torque functional and symmetry theory. Furthermore, an oscillatory trend in the relative magnitudes of the torques between the two vorticity axes is also observed; however, the trend in the relative magnitudes is reversed from that predicted by the functional. The reason for this discrepancy is not clear. Finally, the overall magnitude of the torque is observed to decay rapidly with increasing denominator frequency, corresponding to an increasing number of Lissajous domains.

Two sequences approaching unity were investigated as well. The first consists of irreducible ratios containing an even integer, $[k/(k+1),\ k=1,2,\ldots]$, and the second consists of only odd numbers, $[(2k-1)/(2k+1),\ k=1,2,\ldots]$. Fig. 5(a) shows that for the even, odd field sequence there is an oscillation between the torque being around the low and high frequency axis, as expected from symmetry theory, and that the maximum torque is again asymptotically scaling as the inverse number of domains in the Lissajous plot. For odd:odd fields the torque is predicted to occur only around the dc field direction and once again it falls off as the inverse

number of domains, Fig. 5(b), but the amplitude is much larger for any given domain number than for the other cases investigated.

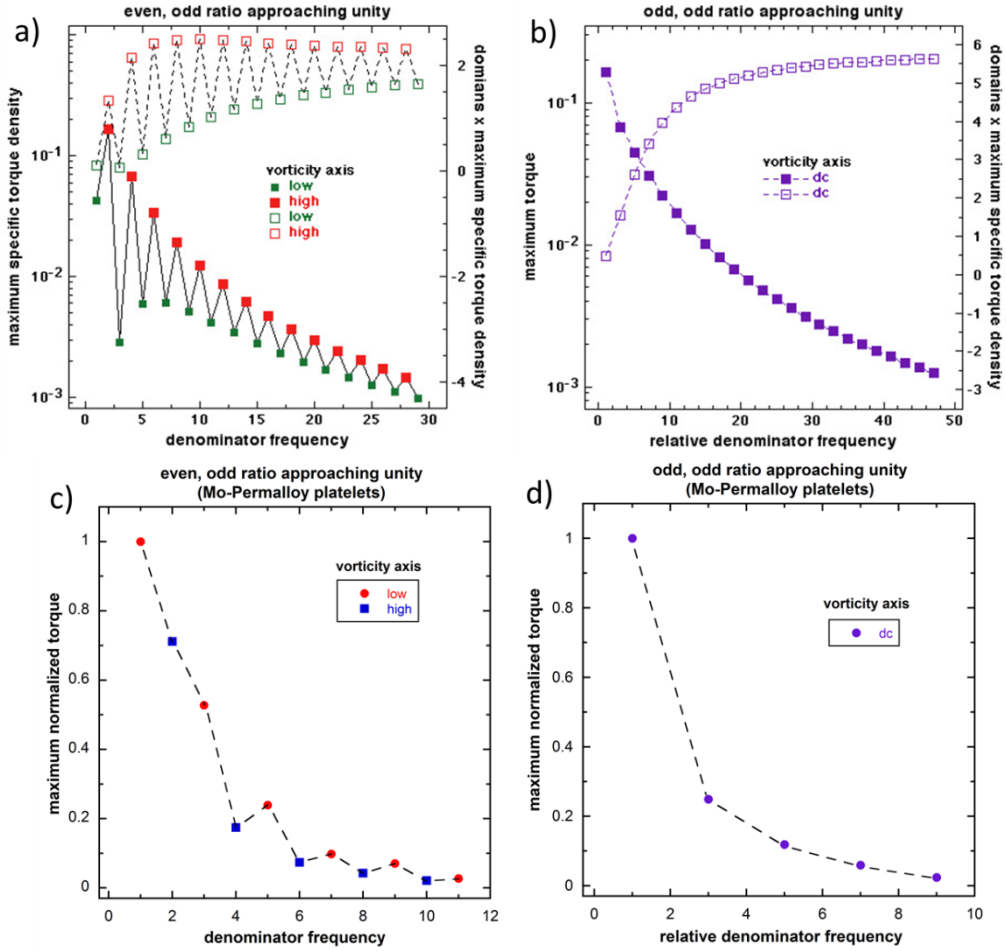

Figure 5. The maximum of the torque functional as a function of phase is plotted versus the relative denominator frequency for even:odd and odd:odd frequencies approaching unity. Multiplying these peak torques by the number of domains in the 2-d Lissajous plots shows an approach to an asymptote, indicating an algebraic decay. The odd:odd torques are expected to be especially strong. (bottom) Experimental torque data for even, odd ratio approaching unity. An oscillatory series of torques are produced whose vorticity axis alternates between the high and low frequency components. The magnitude of the torque is observed to decay rapidly as the number of Lissajous domains increases.

Experimental torque data were also collected for the even, odd sequence approaching unity, Figs. 5(c) & (d). In accord with the predicted data from the functional in Fig. 5(a), the experimental torque values display an oscillatory behavior as the overall magnitude rapidly decays with increasing denominator frequency. The oscillations in torque correspond to the vorticity axis alternating between the high and low frequency components. However, as was observed with the sequences approaching ½ from above and below, the trend in the relative magnitudes between the two vorticity axes is reversed from that predicted by the functional. The odd:odd ratio approaching unity was also investigated, Fig. 5(d), in which case the torque only occurs around the dc field axis and falls off rapidly with increasing denominator frequency.

Finally, neighboring terms in a Fibonacci sequence are relative primes and so make sequences of irreducible rational numbers. We investigated the sequence 1:1, 1:2, 2:3, 3:5, 5:8, 8:13,… This sequence approaches the inverse golden ratio. The maximum torque functional for this sequence is plotted in Fig. 6. The vorticity axis is observed to form the repeated axis

sequence dc, low, high, which is once again in accord with symmetry theory. Once again the torque falls off as the inverse number of domains in the Lissajous plots.

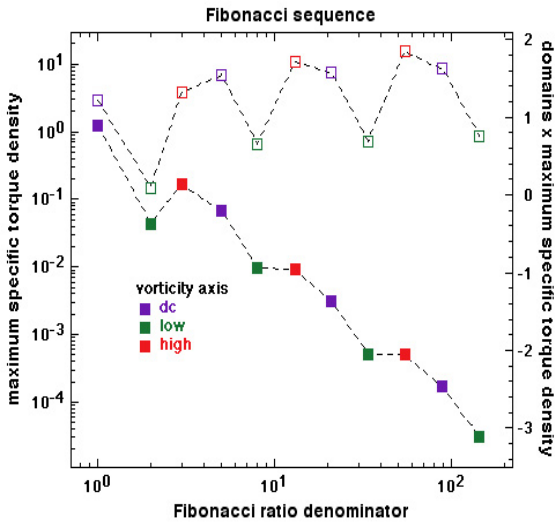

Figure 6. The Fibonacci sequence creates a periodic transition
between all three field axes and once again the peak torque falls off as the inverse of the number of domains.

3.5. Flow Reversal

In a previous publication [8] we reported a very strange observation for a 1:2 field. After applying the ac fields the dc field was slowly ramped up, which caused fluid vorticity to initiate and progressively increase. As the field was progressively increased further the vorticity slowed down, stopped, and then reversed direction. Symmetry theory cannot address this issue, but can the torque functional shed light on this? In Fig. 7 calculations are shown for a 1:2 field over a range of dc field strengths, ranging from $c = 0$ to 1.25 (see Eq. 3). Flow reversal occurs at roughly $c = 0.75$, which is commensurate with experimental observations of surface flow [8]. We pursued this issue by investigating many different symmetry-breaking fields and for all fields of the form odd:odd + 1 that we have investigated flow reversal is indicated. We can find no other fields where the torque functional indicates flow reversal.

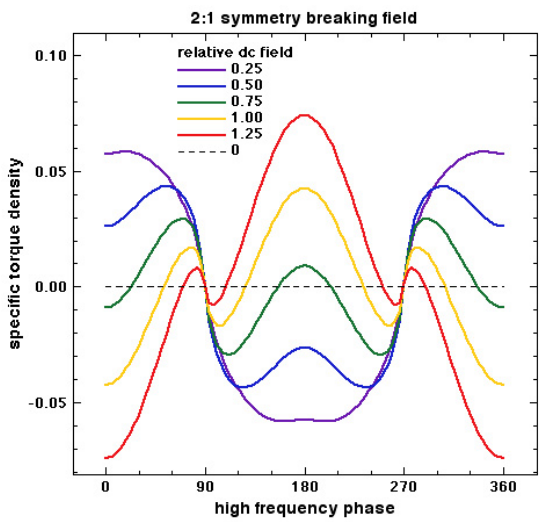

Figure 7. For all of the odd:odd+1:dc fields we have investigated (1:2, 3:4,…)
the torque functional indicates flow reversal with increasing field. Flow reversal seems to be unique to this class of fields.

3.6. Inducing Vorticity with Biaxial Fields?

It is quick and easy to investigate a lot of ideas with the torque functional, including ideas that might be difficult to screen experimentally. Symmetry-breaking rational fields consist of three orthogonal components and thus are three-dimensional fields. Is it possible to initiate strong vorticity with fields confined to a plane? Take for example the biaxial field in the *x*-*y* plane with frequency ratio 2:3. Recall that this field produces vorticity around the *y* axis when a dc field is applied along the *z* axis. If instead a dc field is applied along the *y* axis, which is the odd axis, the torque functional indicates torque around the *z* axis, Fig. 8. The dependence of the torque functional on phase angle approaches a square wave, which is striking. The *z* axis is a C_2 symmetry axis for this case when one considers the equivalency of the field and its converse and the other two axes are antisymmetric under a 180° rotation. Because this symmetry is shared by vorticity around the *z* axis this observation could have been anticipated. Experiments on platelet suspensions do indeed confirm this prediction. On the other hand, if a dc field is applied along the *x* axis the torque functional predicts that vorticity will not occur, and it is notable that all three axes are C_2 axes for the field and its converse, which is not the symmetry of vorticity.

Similar observations apply to the 1:2 field: when a dc field is applied along the odd axis (which in this case is the low frequency axis) the torque functional indicates torque around the *z* axis. When a dc field is applied along the even axis the functional predicts no torque. Again, this behavior could have been anticipated from the symmetry of the trajectories. It would appear that all even, odd fields are capable of producing a *z* axis torque when a dc field is applied along the odd field component.

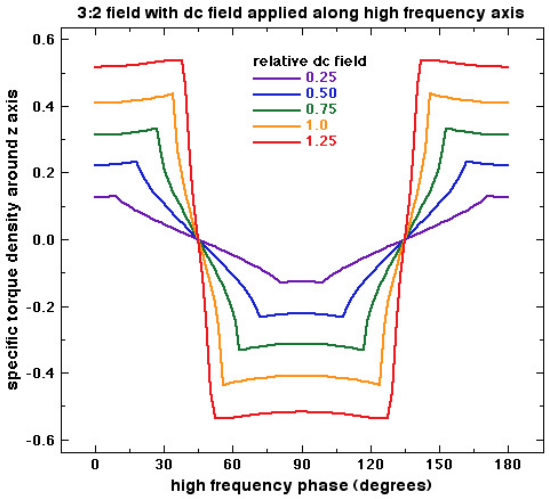

Figure 8. When a dc field is applied along the high frequency axis of a 2:3 field the resulting biaxial field produces torque around the normal to the field plane.

As discussed above, odd:odd fields produce torque around the *z* axis even in the absence of a dc field, because odd:odd fields possess the symmetry of vorticity, with the *z* axis being the C_2 axis of symmetry. Applying a dc field along either of the ac components does not change this symmetry and does not appreciably alter the dependence of the torque functional on phase angle. Odd:odd fields do not seem to be interesting as regards the addition of in-plane dc fields. However, suspensions of spherical particles have a strong tendency to form particle sheets, and the dc field component reduces this tendency, allowing the particles to form the chains that presumably give rise to the torque.

3.7. Rational Triads

The experimental investigation of the torque generated by rational triads is time consuming because there are two independent phase angles. If torque measurements are made at 10° intervals for each of the two phase angles over 1200 measurements are required. At roughly 5 minutes per measurement that requires 100 hrs. of continuous work. Any new ideas about rational fields are therefore tough to sort through, especially those that might lead to off-axis vorticity (see below), which could triple the measurement time, since measurements would in general have to be made along all three field directions. In contrast, it is a matter of much less than a minute to compute the torque functional for the same set of phase angles. These results are sufficiently useful to guide experimental work. In the following we will explore the torque density functional for the specific cases of the four classes of rational triads, three of which we have previously investigated experimentally [11].

In previous work we have shown that there are four classes of rational triads [11]. The first is even, odd, odd and 1:2:3 is the simplest example of this class. Symmetry theory shows that this field produces vorticity around the even axis. The second class is even, even, odd fields with even:even factoring to even:odd. A simple example of this class is 2:3:4 and symmetry theory shows that vorticity is around the odd axis for this class (*i.e.*, "3" in this case). The third class is even, even, odd with even:even factoring to odd:odd and once again symmetry theory predicts vorticity around the odd axis. The example of this class that was experimentally investigated in our previous paper is 1:2:6. Finally, the fourth class is odd:odd:odd, for which symmetry theory could not make predictions, simply because fields of this class do not have the symmetry of vorticity. These fields can be treated by the torque density functional, however, which we will find predicts off-axis vorticity for the example field 1:3:5.

The symmetry theory for rational triads is based on those 3-d Lissajous trajectories that have highly symmetric projections on faces normal to each of the three field directions. These symmetric 3-d trajectories can be expressed by assigning to each of the three sine terms in Eq. 4 one of the phases 0°, 90°, 180°, 270°, corresponding to sine, cosine, −sine, −cosine. There are thus $4 \times 4 \times 4 = 64$ symmetric 3-d Lissajous trajectories that can be treated by symmetry theory. These 64 trajectories can be classified into 4 groups of 16. In each of these groups the magnitude of the torque density is fixed, but 8 of the trajectories give clockwise flow and 8 give counterclockwise. In addition to predicting the vorticity axis symmetry theory also predicts these groups and the relative vorticity sign for each trajectory within each group.

The 1:2:3 triad—Calculations for the 1:2:3 field show that vorticity does indeed occur around the even axis. In Fig. 9 calculations are presented for the torque functional as a function of each possible set of two independent phase angles, (ϕ_1, ϕ_2), (ϕ_2, ϕ_3) and (ϕ_1, ϕ_3). Of course, all of these data sets contain the same information and can be related to each other by a change of variables. For the 1:2:3 field the equivalent phase angles are

$$(\phi_1,\ \phi_2,\ 0),\ (\phi_1 - \tfrac{1}{2}\phi_2,\ 0,\ -\tfrac{3}{2}\phi_2),\ (0,\ \phi_2 - 2\phi_1,\ -3\phi_1).$$

In the (ϕ_1, ϕ_2) plane one lattice vector that defines the unit cell (a vector that preserves torque density) is seen from Fig. 9(a) to be **A**=(0°, 180°). Substituting this phase shift into Eq. 4 (with $\phi_3 = 0$) gives

$$\mathbf{h}(t) = \frac{\mathbf{H}_0(t)}{H_0} = -\cos(ls' + \phi_l)\hat{\mathbf{x}} + \sin(ms' + \phi_m)\hat{\mathbf{y}} + \cos(ns')\hat{\mathbf{z}} \tag{5}$$

where $s' = s + 90°$. The torque equivalence of the fields [−C, S, C] {abbreviation for [−cos(1*s*), sin(2*s*), cos(3*s*)]} and [S, S, S], is in accord with symmetry theory, as shown in Table 5 of

Reference 11. The second lattice vector is $\mathbf{B} = (120°, 60°)$. The change of variables $s' = s + 30°$ leads to [C, S, −C], which is also shown by symmetry theory to be equivalent to [S, S, S]. Experimental data need only be taken over this unit cell, which is only 1/6-th the computed area. The lattice vectors are those phase changes that preserve vorticity. To reverse vorticity at constant magnitude requires a phase change of (60°, 120°).

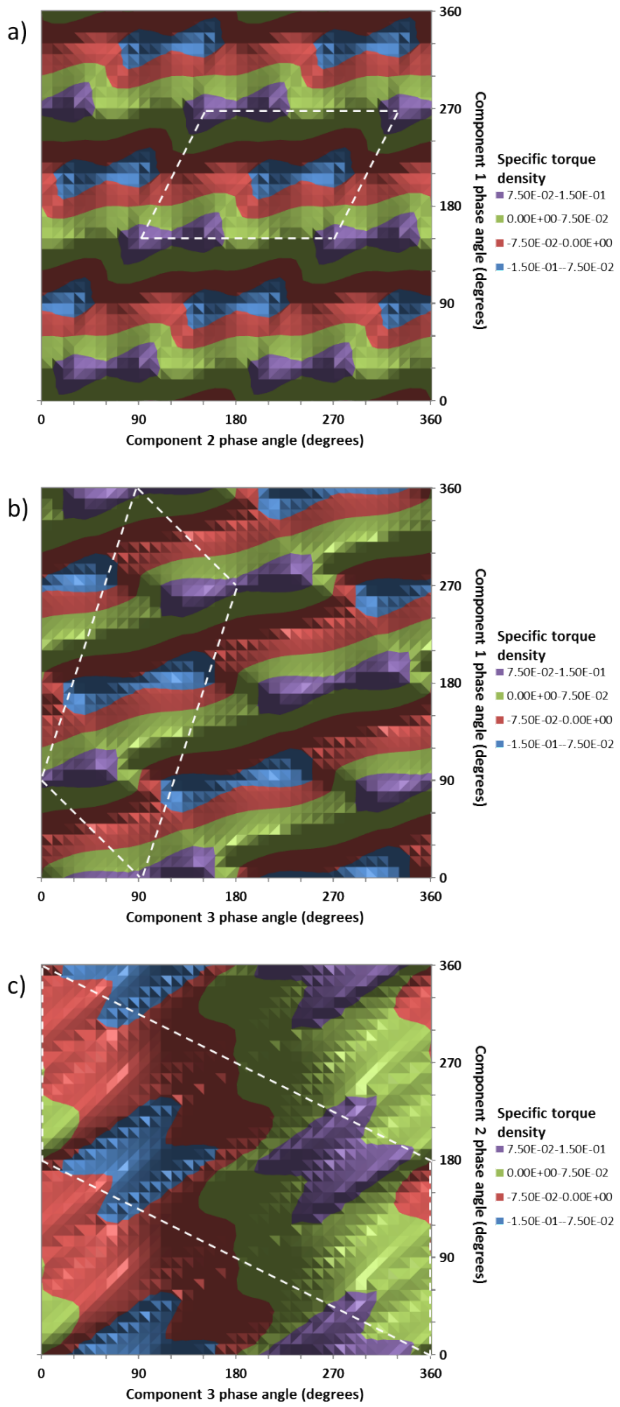

Figure 9. The torque functional correctly predicts torque
around the *y* axis for the 1:2:3 field. Here this torque density is plotted as a function of the three possible sets of phases.

It is interesting to examine how the unit cell transforms in other data planes. For the (ϕ_1, ϕ_3) plane the lattice vectors **A** and **B** become (270°, 90°) and (90°, −90°), which is the rather large and experimentally awkward unit cell observed in Fig. 9(b). In the (ϕ_2, ϕ_3) plane the lattice vectors **A** and **B** transform to (180°, 0°) and (−180°, 360°) to create the unit cell apparent in Fig.

9(c). (Of course, a simpler choice for the unit cell is the lower half of the plane.) In any case, the torque functional can determine which pair of phase shifts leads to a unit cell suitable for experimental investigation, and avoids the issue of taking redundant data. In the (ϕ_1, ϕ_3) plane flow reversal at constant magnitude requires a phase shift of (90°, 90°) and in the (ϕ_2, ϕ_3) the required phase shift is (0°, 180°).

The torque functional can also be computed for the exact phases of all of the 64 symmetric 3-d Lissajous trajectories presented in Table 5 of Reference 11. These computations show that within each group of 16 fields the torque magnitude is indeed constant and the computed relative vorticity signs (CW or CCW) are in agreement as well.

The 2:3:4 triad — In this case the torque functional shows torque around the odd axis ("3"), in accord with the predictions of symmetry theory. The equivalent phase angles are (ϕ_2, ϕ_3, 0), ($\phi_2 - \frac{2}{3}\phi_3$, 0, $-\frac{4}{3}\phi_3$), (0, $\phi_3 - \frac{3}{2}\phi_2$, $-2\phi_2$) and in the (ϕ_2, ϕ_3) plane lattice vectors are **A**=(0°, 180°) and **B**=(90°, 45°), Fig. 10(a). These phase shifts transform [S, S, S] to [S, −S, S] and [S, −C, −S], respectively. Table 1 of the Electronic Supplementary Information (ESI) for Reference 11, shows that symmetry theory shows the equivalence of [S, S, S], [S, −S, S], and [C, −S, −S]. Moreover, torque functional calculations for the 64 symmetric Lissajous trajectories within this table are in agreement with the vorticity magnitude and sign groupings. Flow reversal at constant magnitude can be achieved by the phase change (0°, 90°).

The lattice vectors **A** and **B** become (120°, 240°) and (60°, −60°) in the (ϕ_2, ϕ_4) plane and the unit cell in this case is shown in Fig. 10(b). Flow reversal at constant magnitude can be achieved from the phase change (0°, 180°). In the (ϕ_3, ϕ_4) plane the lattice vectors become (180°, 0°) and (90°, 180°) and a unit cell corresponding to these vectors is shown in Fig. 10(c). The simplest flow reversal vector in this plane is (90°, 0°).

Previously reported experimental data were collected in the (ϕ_2, ϕ_3) plane, which was perhaps not the best choice. The symmetry of these data reflect that of the torque functional, but both the shape of the maxima and their exact locations differ somewhat.

The 1:2:6 triad — This is the final example of a rational field for which we previously collected experimental data. Once again the torque functional demonstrates torque around the axis predicted by symmetry theory, which in this case is the odd axis. The computed magnitudes and the signs of the vorticity are in accord with the predictions of symmetry theory given in Table 2 of the ESI for Reference 11. In the (ϕ_1, ϕ_6) plane the lattice vectors are (0°, 360°) and (90°, 0°), which transform [S, S, S] to [S, S, S] and [C, S, S] respectively. Table 2 of the ESI for Reference 11 shows that symmetry theory predicts that the torque density will be invariant for these fields. Flow reversal at constant magnitude can be achieved with the phase change (0°, 180°). The equivalent phase angles are (ϕ_1, 0, ϕ_6), ($\phi_1 - \frac{1}{6}\phi_6$, $-\frac{1}{3}\phi_6$, 0), (0, $-2\phi_1$, $\phi_6 - 6\phi_1$). In the (ϕ_1, ϕ_2) plane the lattice vectors transform to (60°, 120°) and (90°, 0°). In the (ϕ_2, ϕ_6) plane the lattice vectors become (0°, 360°) and (180°, 540°). The unit cells for each of these representations are evident in Fig. 11. Previously reported experimental data were taken in the (ϕ_1, ϕ_6) plane. These data reflect the symmetry of the torque functional, but the peak torques occur at somewhat different phase angles, demonstrating the limitations of the torque functional.

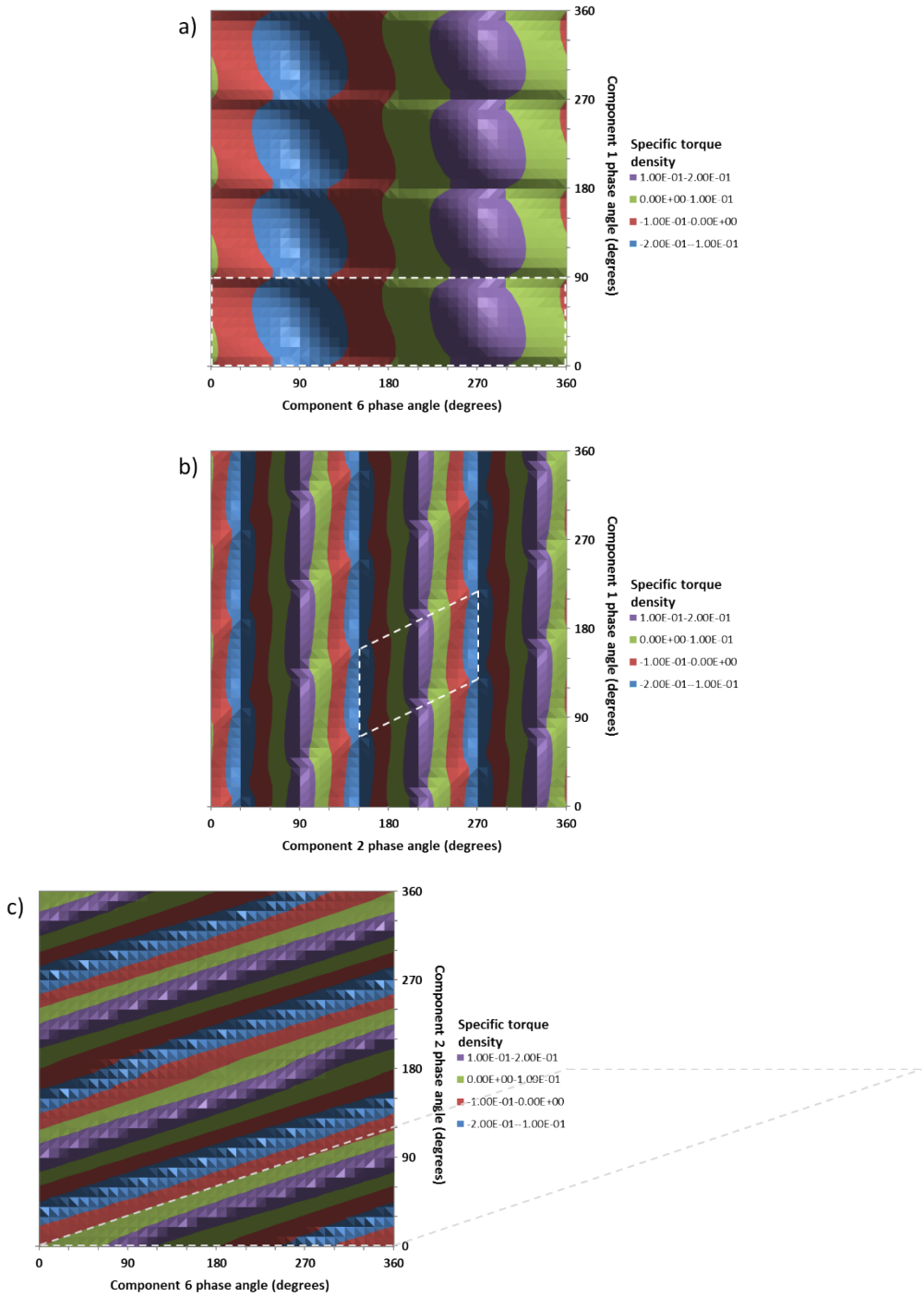

Figure 10. The torque functional correctly predicts torque around the *x* axis for the 1:2:6 field. Again the torque density is plotted as a function of the three possible sets of phases.

The 1:3:5 triad—Odd:odd:odd fields do not have the symmetry of vorticity and so we could not conclude anything about the torque created by these fields in our previous paper [11]. However, some interesting comments can be made about such fields. Recall that for symmetry-breaking, odd:odd fields the vorticity is invariant to the direction of the dc field. This fact implies that if the dc field is replaced by an alternating field fluid vorticity will still occur around the same axis. Indeed, odd:odd:dc and odd:odd:even both produce vorticity around the *z* axis. However, by the same logic odd:odd:odd fields should produce vorticity around all axes, so the situation is one of competing amplitudes, which is the domain of the torque functional.

For the 1:3:5 field the torque functional predicts torque around all field directions, so the net torque will be off axis. The computed torques around the x, y, and z axes are shown in Fig. 12. Under the qualitative reasoning of the previous paragraph torque around the x axis is produced by the 3,5 components. The torque functional peaks at 0.175 for this axis. The torque functional around the z axis peaks at 0.081 and can be roughly thought of as being created by the 1,3 components. Finally, the torque functional around the y axis peaks at only 0.0033 and can be approximately attributed to the 1,5 components. In fact, calculations for the balanced symmetry breaking field 1:3 produces a torque maximum of 0.163, for 3:5 the maximum is 0.067 and 1:5 maximizes at 0.002. The torque around the y axis is too small to measure, but the other torques were mapped out in the (ϕ_1, ϕ_5) plane, Fig. 13.

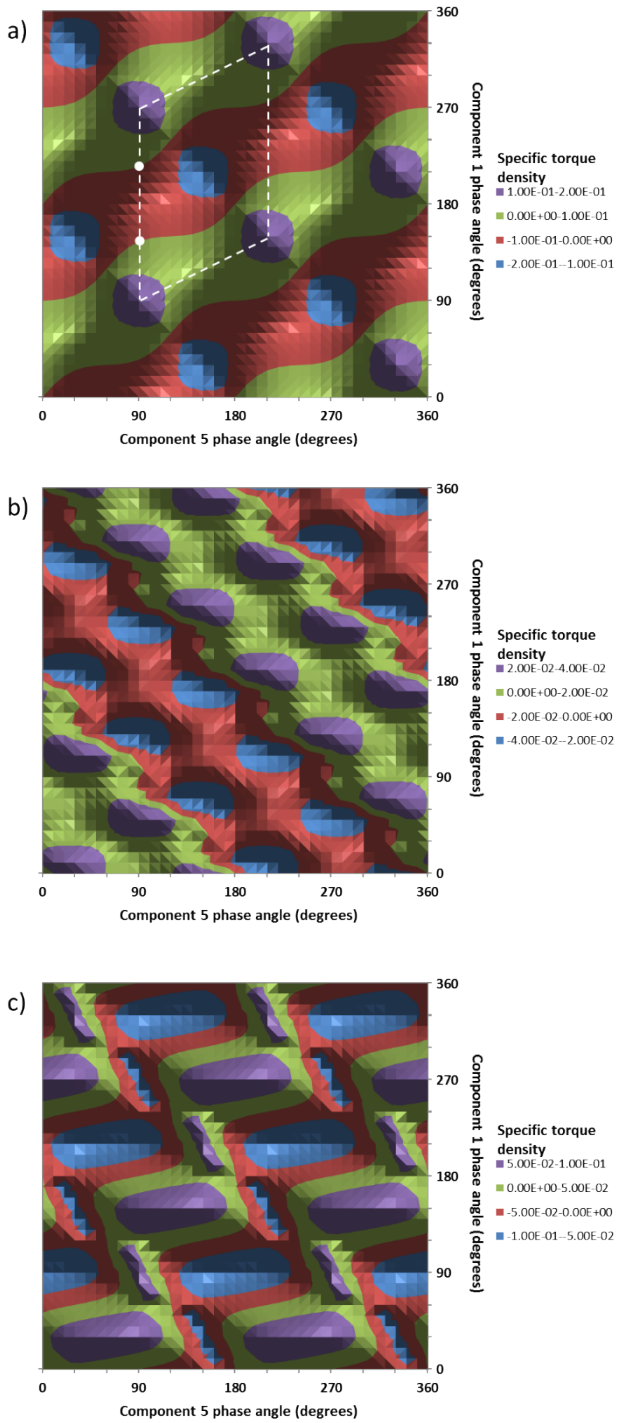

Figure 11. The torque functional predicts torque around all axes
for the 1:3:5 field: (a) around the x axis; (b) around the y axis; and (c) around the z axis.

Although the experimental torque data almost appear sheared or skewed compared to those predicted by the functional in Fig. 12(a), both sets possess the same unit cell defined by the lattice vectors (180°, 0°) and (60°, 120°). Despite the fact that both sets of data possess the same *symmetry*, there is a phase shift between the predicted and experimental data indicated by the fact that the positions of the extrema are not in the exact same location in each phase map. The origin of this phase offset is not clear at this time, but was also seen with previously studied rational triads (*i.e.*, 1:2:3, 1:2:6, and 2:3:4) [11].

There is a noteworthy consequence concerning *flow reversal* due to the subtle differences between the experimental data, which appear sheared, compared to those predicted by the functional. Recall that the locus of points that delineate the green and red regions in these torque density maps are points of *zero torque*, and thus indicate points of flow reversal. In both the predicted and experimental phase maps [Figs. 12(a) & 13], points of flow reversal are indicated by white dots on the boundary of the unit cell. The torque functional predicts no points of flow reversal on the canted boundaries and two points on the vertical boundaries; whereas, experiments reveal two points of flow reversal on the canted boundaries and four on the vertical boundaries.

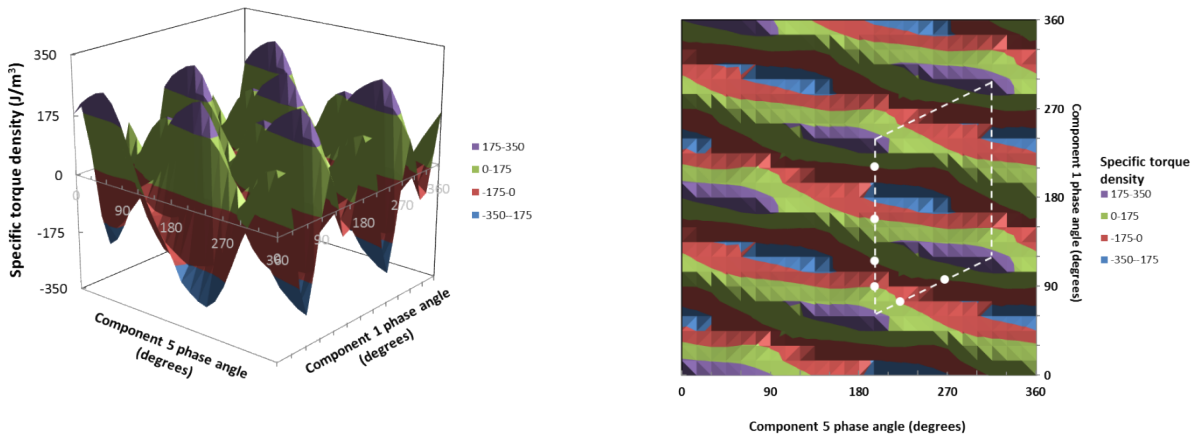

Figure 12. The torque functional predicts torque around all axes for the 1:3:5 field:
(a) around the *x* axis; (b) around the *y* axis; and (c) around the *z* axis.

4. SUMMARY

We have developed a functional—by using physical insight and previous results based on the theory of vortex magnetic field mixing—that can be used to predict the relative *magnitude* and direction of the vorticity vector in magnetic particle suspensions driven by complex, time-dependent magnetic fields (symmetry-breaking rational fields and rational triads). We find that the functional predicts results that are in agreement with both the symmetry theories developed for these new classes of fields as well as experimental observations. Such a functional allows for the rapid investigation of innumerable magnetic field schemes, which can be used to direct future experimental work, and serves as a natural first step toward understanding the microscopic origins of the observed vorticity. Experimental results are given for a wide variety of symmetry-breaking fields, showing that the torque density falls off rapidly as the number of domains in the Lissajous plot increases. The 1:3:5 rational field was investigated experimentally and gives good agreement with the predictions of the torque functional. The vorticity direction produced by this field cannot be predicted by symmetry theory, but the torque density functional shows that the vorticity axis is not aligned with any of the three field components, and this is indeed the experimental observation.

CREATING ORBITING VORTICITY VECTORS IN MAGNETIC PARTICLE SUSPENSIONS THROUGH FIELD SYMMETRY TRANSITIONS — A ROUTE TO MULTI-AXIS MIXING

5. INTRODUCTION TO VORTICITY ORBITS

We have recently reported that two types of triaxial electric or magnetic fields can drive vorticity in dielectric or magnetic particle suspensions, respectively. The first type — *symmetry-breaking rational fields* — consists of three mutually orthogonal fields, two alternating and one dc, and the second type — *rational triads* — consists of three mutually orthogonal alternating fields. In each case it can be shown through experiment and theory that the vorticity vector is parallel to one of the three field components. For any given set of field frequencies only one vorticity direction is possible, but the sign and magnitude of the vorticity (at constant field strength) can be controlled by the relative phase angles and, at least for some symmetry-breaking rational fields, the direction of the dc field. In short, the locus of possible vorticity vectors is a 1-d set that is symmetric about zero is along a field direction. In this paper, we show that continuous 3-d control of the vorticity vector is possible. The trick is to progressively transition the field symmetry by applying a dc bias along one of the principal axes of a rational triad while keeping the rms field amplitude constant along that axis. Such *biased rational triads* are intermediate between symmetry-breaking rational fields and rational triads. A surprising aspect of these transitions is that the locus of possible vorticity vectors for any given field bias is extremely complex, encompassing all three spatial dimensions. As a result, the trajectory of a vorticity vector as the dc bias is increased is complex, with large components occurring along unexpected directions. More remarkable are the braided vorticity vector orbits that occur when one or more of the field frequencies are detuned. These orbits provide the basis for highly effective mixing strategies. Both numerical computations and experimental data are presented.

In this chapter we demonstrate that it is possible to use alternating triaxial magnetic fields to produce complex noncontact mixing in fluids seeded with very small volume fractions of magnetic particles. In many mixing processes, such as those produced by stirring, fluid vorticity occurs around just a single axis. This might not be the optimal approach for complex volumes, such as those that can occur in engineered microfluidic systems. And this might not be the optimal approach for heat transfer applications with complex boundaries. We have discovered that dc biasing certain alternating triaxial fields produces extremely complex mixing processes when one or more of the field components is phase modulated. In many cases the resultant vorticity vector never vanishes, but undergoes elaborate trajectories through all three spatial dimensions. These trajectories can be varied over an enormous range by detuning multiple field components. The results in this paper could be exploited to create entirely new approaches to efficient mixing and heat transfer in complex geometries.

In the last few years it has been shown that a wide variety of triaxial magnetic fields can produce strong fluid vorticity. These fields are comprised of three mutually orthogonal field components, of which, either two or three are alternating, and the various frequency ratios are rational numbers. These dynamic fields generally lack circulation, in that a soft ferromagnetic rod subjected to one of these fields does not undergo a net rotation during a field cycle. Yet these fields do induce *deterministic* vorticity, which might seem counterintuitive. This vorticity is not a parity violation because the field trajectory, considered jointly with its physically equivalent converse, has parity. Parity occurs because the symmetry of this pair of fields is shared by vorticity: reversing this parity reverses flow. An analysis of the symmetry of these fields enables the prediction of the vorticity axis, which is determined solely by the relative frequencies of the triaxial field components.

Changing the relative *phases* of the field components enables control of the magnitude and sign of the vorticity, and in some cases changing the direction of the dc field also reverses flow. When the frequency of one of the field components is detuned slightly, a slow modulation of the relative phase occurs. This heterodyning causes the flow to periodically reverse, but it remains on a single axis. Such flows produce a simple form of stirring. Certain triaxial fields produce unexpected changes in the direction of the vorticity vector when a dc field is applied along one of the ac field components, because the dc field causes a transition in the symmetry of the triaxial field. Heterodyning one or more of the field components in such a *biased rational triad field* is the key to creating the aforementioned elaborate vorticity orbits.

6. FIELD SYMMETRY TRANSITIONS

Understanding the rational for investigating field-symmetry transitions requires a little background. We have discovered two methods of inducing fluid vorticity in magnetic particle suspensions. In the first method two orthogonal ac components whose frequency ratio is a rational number are applied to the suspension. Vorticity is induced when an orthogonal dc field is applied, because this field creates the parity needed for deterministic vorticity. We have developed a theory of these *Symmetry-Breaking Fields* that predicts the direction and sign of vorticity as functions of the frequencies and phase. The second method is based on *Rational Triads,* fields comprised three orthogonal ac fields whose relative frequencies are rational (e.g. 1:2:3). These fields can also permit vorticity and we have developed a symmetry theory that allows us to compute the direction and sign of vorticity as functions of the frequencies and phases. By progressively changing one of the ac components of a rational triad to dc we will generate competing symmetries that should lead to a continuous reorientation of the vorticity vector, providing fully 3-d control of fluid vorticity.

Our approach is based on the discovery that both ac/ac/dc and ac/ac/ac fields can generate fluid vorticity. The axis around which this vorticity occurs is the critical factor for the concept of field-symmetry-driven vorticity transitions. For the ac/ac/dc Symmetry-Breaking Fields the vorticity axis is determined by the ratio *l:m* of the two ac frequencies. If *l* and *m* are relatively prime then at least one of these numbers is odd. A consideration of the joint symmetry of the field and its converse shows that if only one of these numbers is odd the vorticity is parallel to the odd field component and reversing the dc field reverses the vorticity. If both of these numbers are odd the vorticity is parallel to the dc field component. For odd:odd fields reversing the dc field direction does not reverse the flow, which suggests that for these fields the dc field component can be replaced by an ac field and vorticity can still occur (the truth is a little more complicated—see discussion below). In all cases the sign and magnitude of the vorticity can be controlled by the phase angle between the ac components.

For the fully alternating Rational Triad Fields the direction of vorticity is controlled by the three relative field frequencies *l:m:n*, where *l*, *m* and *n* are integers having no common factors. There are four classes of such fields: I) even:odd:odd; II) even:even:odd where even:even can be factored to even:odd; III) even:even:odd where even:even can be factored to odd:odd and; IV) odd:odd:odd. By analyzing the joint symmetries of the 3-d Lissajous trajectories of the field and its converse it is possible to show that the direction of vorticity is parallel to the field component that has unique numerical parity. The fourth class (odd:odd:odd) has no component with a unique numerical parity and does not possess the symmetry required to predict a vorticity axis.

Consider now the possibility of creating a continuous symmetry transition by gradually transitioning one of the three ac field components into a dc field, while keeping the rms field amplitude constant. To be definite we will let *l*, *m*, and *n* lie along the *x*, *y*, *z* components, respectively. For example, if it desired to transition the *z* component of the field to dc the expression is

$$H_0^{-1}\mathbf{H}_0(t) = \sin(l \times 2\pi ft + \phi_l)\hat{\mathbf{x}} + \sin(m \times 2\pi ft + \phi_m)\hat{\mathbf{y}} + \left[\sqrt{1-c^2}\,\sin(n \times 2\pi ft + \phi_n) + \frac{c}{\sqrt{2}}\right]\hat{\mathbf{z}}\,.$$

In this form all three field components have equal rms values and the ac to dc transition is effected by increasing *c* from 0 to 1 or from 0 to -1. The effect of this ac-dc transition on field symmetry depends on both the type of rational triad and the component that is transitioned.

6.1. Even, Odd, Odd Fields

To be definite we consider the odd:even:odd field 1:2:3, which is shown in Fig. 13(a) for one particular set of phases. For this class of fields the vorticity axis is along the even direction, which in this case is the y axis. If the y field component is continuously transitioned to dc the vorticity axis will remain in the y direction (see the symmetry-derived rules given above), so no rotation of the vorticity axis is anticipated because field symmetry is preserved in this transition. In this particular case the sign of the final vorticity is independent of the sign of the dc field, but is dependent on the phase angles of the ac field components, so a vorticity-reversal transition should be possible wherein the fluid stagnates at some point (value of c) in the transition.

Transitioning the odd field components to dc is much more interesting. If the x component is fully transitioned to dc a change of field symmetry occurs that causes the vorticity vector to reorient from the y to the z axis. The progression of this symmetry change can be seen in Figs. 13(a-d). For intermediate values of the dc amplitude ($0<|c|<1$) the field and its converse do not exhibit the symmetry of vorticity, but the continuous nature of the field transition suggests a continuous reorientation of the vorticity axis nevertheless: it would seem unphysical for the vorticity to simply vanish for intermediate dc field amplitudes. An interesting aspect of this particular field transition is that the final vorticity sign is dependent on the dc field direction. This means there are four possible vorticity axis transitions: one wherein the vorticity axis vector transitions from $+y$ to $+z$, one from $+y$ to $-z$, one from $-y$ to $-z$ and one from $-y$ to $+z$. It is reasonable to assume that the vorticity vector rotates in the y-z plane in all cases, but we will find that this is not the case and very strong vorticity can emerge along the x axis for intermediate dc amplitudes. This unexpected out-of-plane vorticity is investigated below by using the *torque density functional* to compute the torque density for these fields.

The same considerations hold when the z component is continuously transitioned to dc, only in this case the final vorticity axis is along x. We thus expect to be able to orient the vorticity vector anywhere in the x–y plane, but we will see that a strong contribution to the vorticity occurs around the z axis, which is very surprising.

To summarize, for even, odd, odd fields applying a dc field along one odd ac component causes the vorticity to rotate from the even component direction to the other odd component. Applying a dc field along the even component does not cause a change in the vorticity direction.

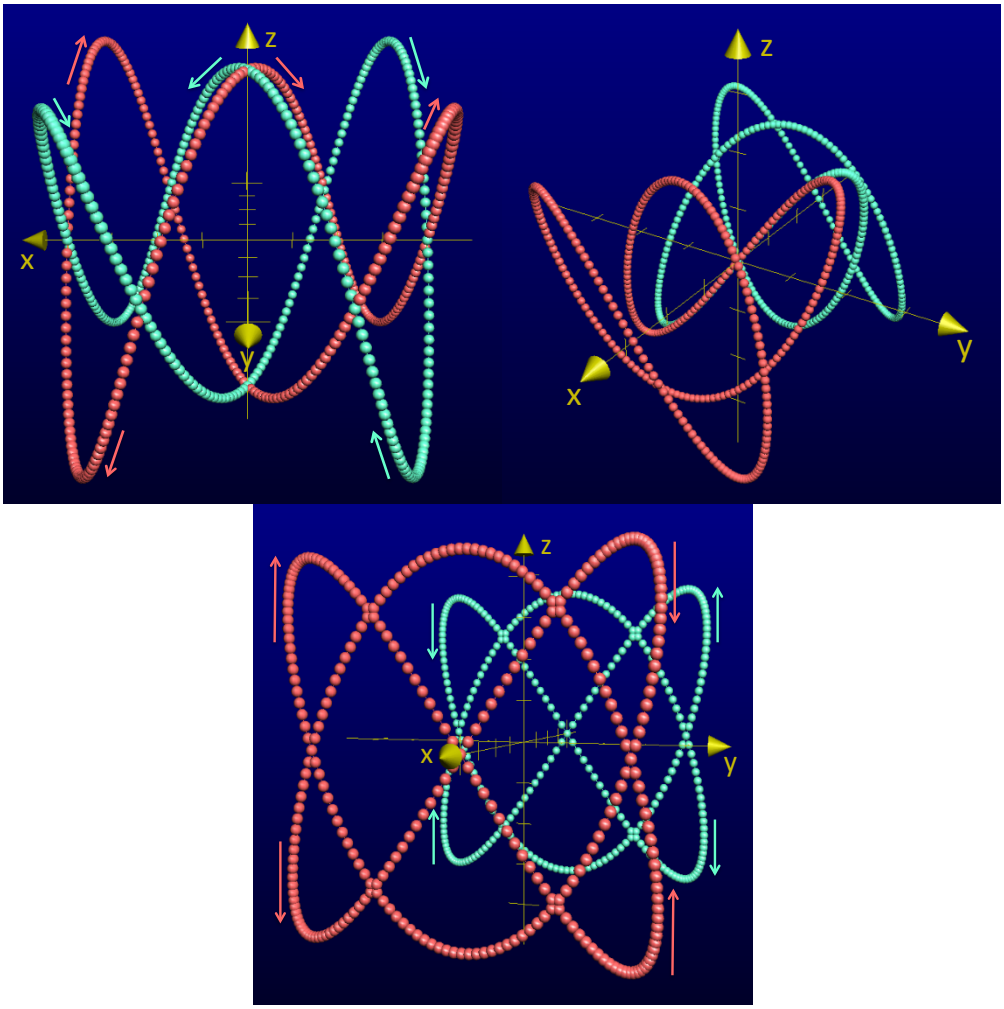

Figure 13. The field symmetry transition is illustrated for the 1+dc:2:3 triaxial field.
In the top left plot the field trajectory and its converse are shown with zero dc bias. The C_2 symmetry axis of this rational triad is the *y* axis, which is the vorticity axis. The *x* and *z* axis are antisymmetric under a 180° rotation. The top right plot has a 50% dc bias along the *x* axis and does not possess the symmetry of vorticity. The bottom plot has 100% dc bias, so the ac amplitude is zero. This is now a symmetry-breaking rational field and the *z* axis is the C_2 symmetry axis and the vorticity direction.

6.2. Odd, Even, Even Fields where Even:Even Factors to Odd:Even

The simplest field of this type is 1:2:4. For these fields the vorticity is around the odd axis, which is *x* in this case. As a result, if the *y* or *z* component of the field is transitioned to dc the direction of the vorticity will not change. The sign of the vorticity might change, however, because in this case it is dependent on the sign of the dc field. Thus a symmetry-driven transition that gives rise to flow reversal can be effected by a proper selection of the dc field sign.

If the *x* component transitions to dc the vorticity axis will reorient from the *x* to the *y* axis, with the vorticity sign again dependent on the dc field sign. In this case it is expected that the vorticity vector can be continuously oriented in the *x*–*y* plane, but once again we will see that the torque density functional predicts a surprising component along the *z* axis during this transition.

In summary, for odd, even, even fields applying a dc field along either even component will not change the orientation of the vorticity axis, but may cause it to reverse. Applying a dc field along the odd component will cause the vorticity to rotate from the odd field axis to the odd axis that arises from factoring even:even.

6.3. Odd, Even, Even Fields where Even:Even Factors to Odd:Odd

For this class of fields, such as 1:2:6, the vorticity is around the odd field axis, which is along x in this case. If one component of such an odd:even:even field is fully transitioned to dc there are three possible outcomes: dc:odd:odd, odd:dc:even, odd:even:dc. In each case the symmetry rules show that the vorticity is around the x axis (underlined). Therefore no change in the orientation of the vorticity is expected, though its sign and magnitude might change during the transition. In other words, such fields produce robust vorticity that is not strongly affected by stray dc fields. Note that only if the even field is transitioned does the final vorticity sign depend on the sign of the dc field.

6.4. Odd:Odd:Odd Fields

The final case of odd:odd:odd fields is interesting, because any field component that is transitioned to dc becomes the vorticity axis. This suggests that applying a dominant dc field in any direction will induce vorticity around that field, enabling fine control of the vorticity direction. But reality is a bit more complex, as discussed below.

6.5. Torque density functional

In the previous chapter we proposed a measure of the torque density of a triaxial field that is based on both theory and experiment. This functional was found to conform to all of the predictions of the symmetry theories but can also be applied to those cases where the trajectories of the triaxial fields do not possess the symmetry of vorticity, such as the field-symmetry-driven vorticity transitions that are the focus of this paper. The functional is given by

$$\mathbf{J}_{\{\phi\}} = \int_0^1 \mathbf{J}_{\{\phi\}}(s)\,ds \text{ where } \mathbf{J}_{\{\phi\}}(s) = \left|\mathbf{h}(s)\right|^2 \frac{\mathbf{h}(s)\times\dot{\mathbf{h}}(s)}{\left|\mathbf{h}(s)\times\dot{\mathbf{h}}(s)\right|} \tag{2}$$

where the dependence on the phase angles is indicated. The torque density is related to this by $\mathbf{T}_{\{\phi\}} = const \times \varphi_p \mu_0 H_0^2 \mathbf{J}_{\{\phi\}}$, where μ_0 is the vacuum permeability and φ_p is the particle volume fraction.

Applying this functional to the 1:2:3 field produces some surprising results. For zero dc field the vorticity is parallel to the y axis (along the "2" field component) and for the full dc case, dc:2:3, it is parallel to the z axis, both in accordance with symmetry theory. For intermediate values of c a simple 'rule of mixing' consistent with a field-squared effect is

$$\mathbf{J}_{\{\phi\}}(c) = (1-c^2)\left|J_{\{\phi\}}(0)\right|\hat{\mathbf{y}} + c^2\left|J_{\{\phi\}}(1)\right|\hat{\mathbf{z}}\,. \tag{3}$$

This expression confines the vorticity vector to the y–z plane, which seems reasonable, but how does this expression compare to the predictions of Eq. 2? It is clear that inserting Eq. 1 into Eq. 2 does not result in an expression in which the ac and dc terms are separable, but it is not clear how important this is.

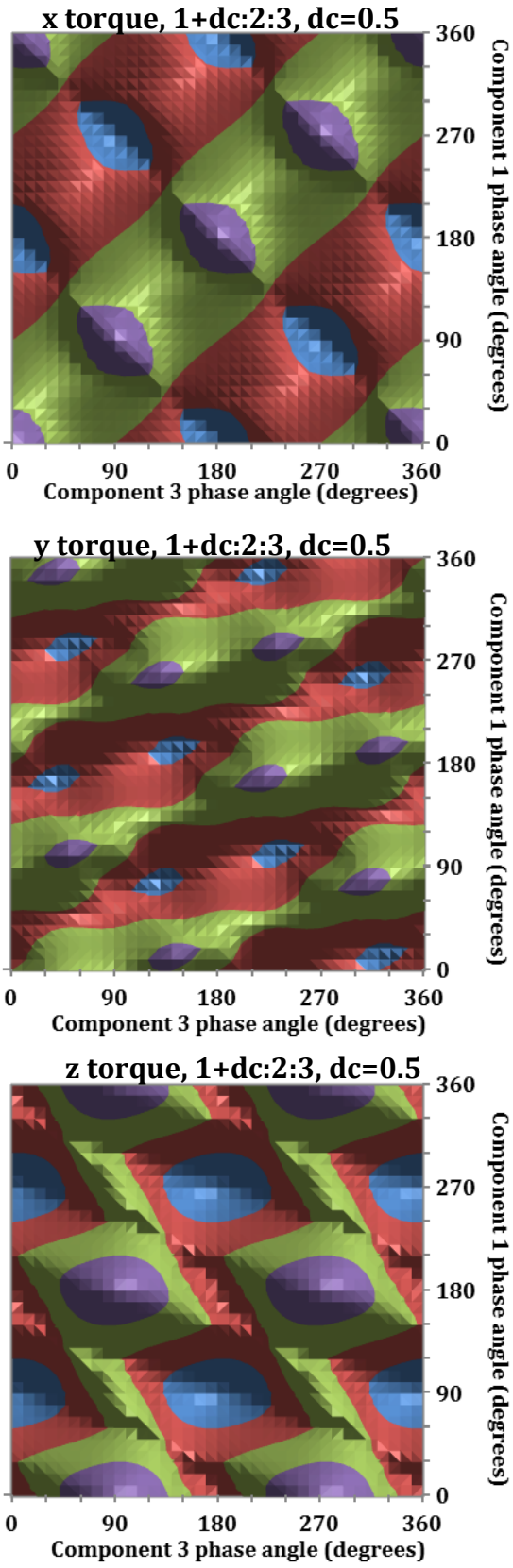

Figure 14. Torque components along all three axes for a 1+dc:2:3 field with a *c*=0.5.

6.6 Predicted torque densities along the three field components

To obtain an appreciation for the complexity of this symmetry transition we have plotted in Fig. 14 components of the torque density computed from Eq. 2 as functions of the phase angles ϕ_1 and ϕ_3 for c=0.5. It is surprising to see that there is a component along the x axis, and in fact this is the dominant component, with a maximum value of 0.16 (arb. units) as compared to 0.09 for the y axis and 0.12 for the z axis.

The nature of the continuous vorticity transition from the rational triad 1:2:3 to the symmetry-breaking rational field dc:2:3 is illustrated in Fig. 15 by plotting the torque density for a square lattice of points in the ϕ_1-ϕ_3 plane, separated by 10° along each cardinal direction. For the rational triad (c=0) the computed torque vectors are along the y axis, so changing the phase angles merely changes the magnitude and sign of the vorticity. But even when a small dc bias is applied along the x axis the torque vectors have comparable components along both the x and z axes. Changing the phase angles thus enables a change in both the magnitude and direction of the fluid vorticity through all three dimensions. As the dc field increases, the torque density data expands, eventually attaining a shape reminiscent of a pendulum ride and finally collapsing onto the z axis when the field along the x axis no longer contains an ac component: this is the symmetry-breaking-field limit, where c=1.

The full range of 3-d control of the torque density is given in Fig. 16, where torque density data for numerous values of the dc bias are plotted, again for the square lattice of phase angles referred to in Fig. 15. The torque density has significant components in the x and z directions and by proper selection of the dc bias and phase angles vorticity can be created along essentially any direction. This complex set of vorticity vectors has many implications for mixing and heat transfer, as we will see.

It is interesting to determine how the torque density produced at any given pair of phase angles evolves as the dc bias is progressively increased. To this purpose we have investigated phase angles along the first three transects shown in Fig. 17. This figure serves as the color key for the curves in Fig. 18. Recall that each of these curves must start on the y axis and terminate on the z axis.

In the top left figure is the result of using the simple mixing law of Eq. 3 to estimate the torque density during the field symmetry transition from 1:2:3 to dc:2:3. Here each line represents a different pair of phase angles along the first transect shown in Fig. 17. For this transect ϕ_1=0° and ϕ_3 increases from 0° to 360° by intervals of 20°. Not all colors in the key are shown because certain phase angles give the same curves when this mixing law is used. Equivalent ϕ_3 angles are (90°+n, 90°-n) and (270°+n, 270°-n) where 0°≤n≤90°. Data are for $0 \le c \le 1$ in intervals of 0.01. This mixing law predicts that the torques are confined to the y-z plane, but the behavior predicted by the torque functional is much more complex.

When the torque functional is used to predict the torque density the result is dramatically different. In Fig. 18 (top right) are shown computations for the phase angles along the first transect. All the colors in the key in Fig. 17 are now shown because each pair of phase angles produces a unique curve. These torque density curves have substantial deviations from the y-z plane and in some cases the x torque is dominant. In all cases if the dc field is reversed ($0 \ge c \ge -1$) both the x and the z torque components are reversed, which constitutes a rotation by 180° around the y axis. Torque density calculations for points along the second and third transects are also given in Fig. 18. Once again, the x component of the torque frequently dominates. Reversing the dc field ($0 \ge c \ge -1$) would fill out the upper hemisphere for torque densities along the second transect, but would do nothing along the third transect. We conclude that, in general, increasing the dc bias is expected to produce a complex evolution of the vorticity.

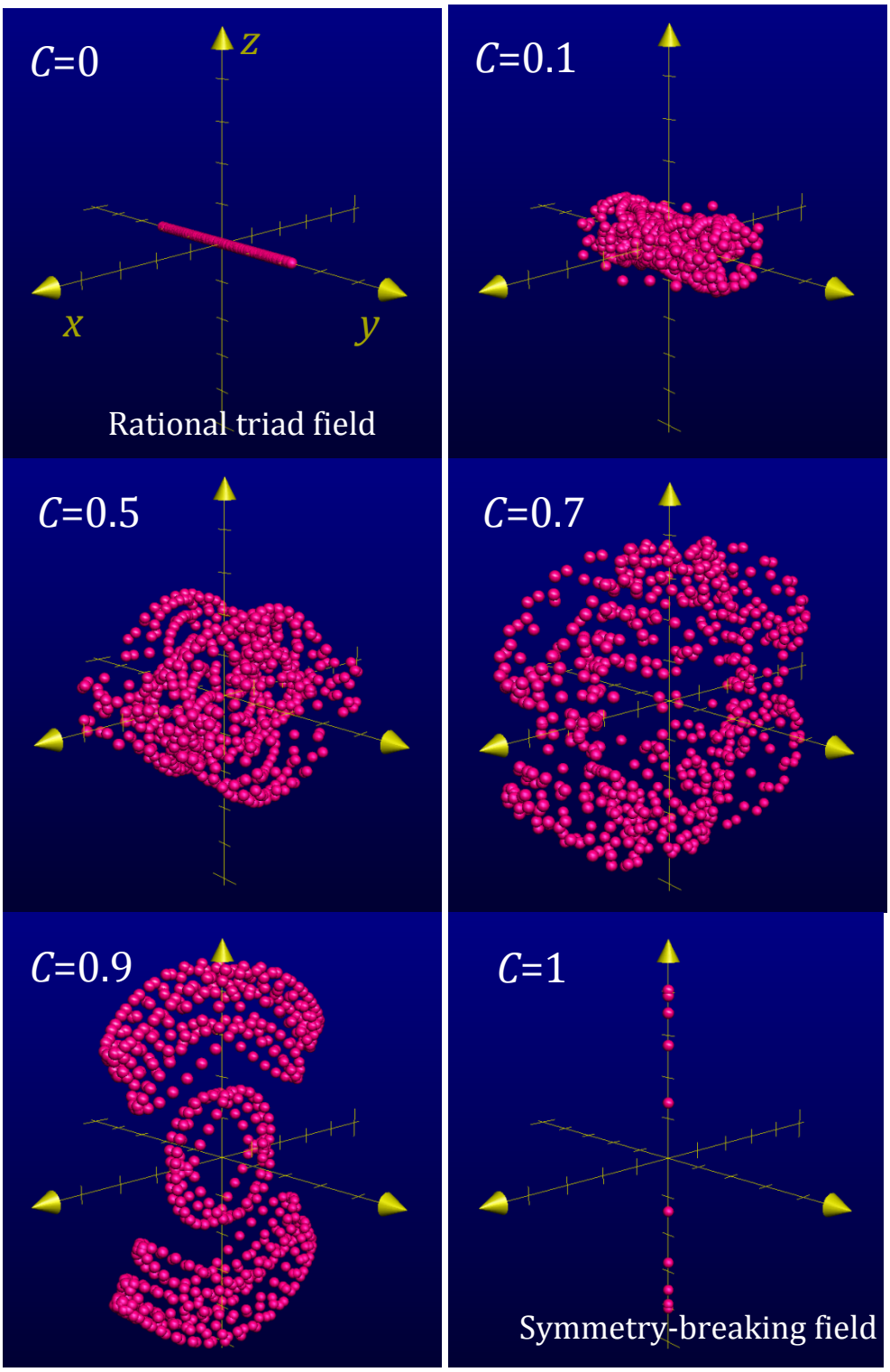

Figure 15. The nature of the continuous vorticity transition from the rational triad 1:2:3 to the symmetry-breaking rational field dc:2:3 is illustrated. These data are the computed torque functional, Eq. 2, for a square lattice of points in the ϕ_1-ϕ_3 plane in Fig. 14, separated by 10° along each cardinal direction. For the rational triad (c=0) the computed torque vectors are along the y axis, so changing the phase angles merely changes the magnitude. When a dc bias is applied along the x axis the torque vectors fairly explode off the y axis to have significant components along both the x and z axes, so changing the phases angles now enables a change in both the magnitude and direction of the fluid vorticity. As the dc field increases, this cloud of torque density data expands into a shape reminiscent of a pendulum ride, finally collapsing onto the *z* axis when the field along the *x* axis no longer contains an ac component: this is the symmetry-breaking-field limit, where *c*=1. Field biasing thus enables continuous control over the direction of the vorticity direction. The tick marks on all axes are separated by 0.025.

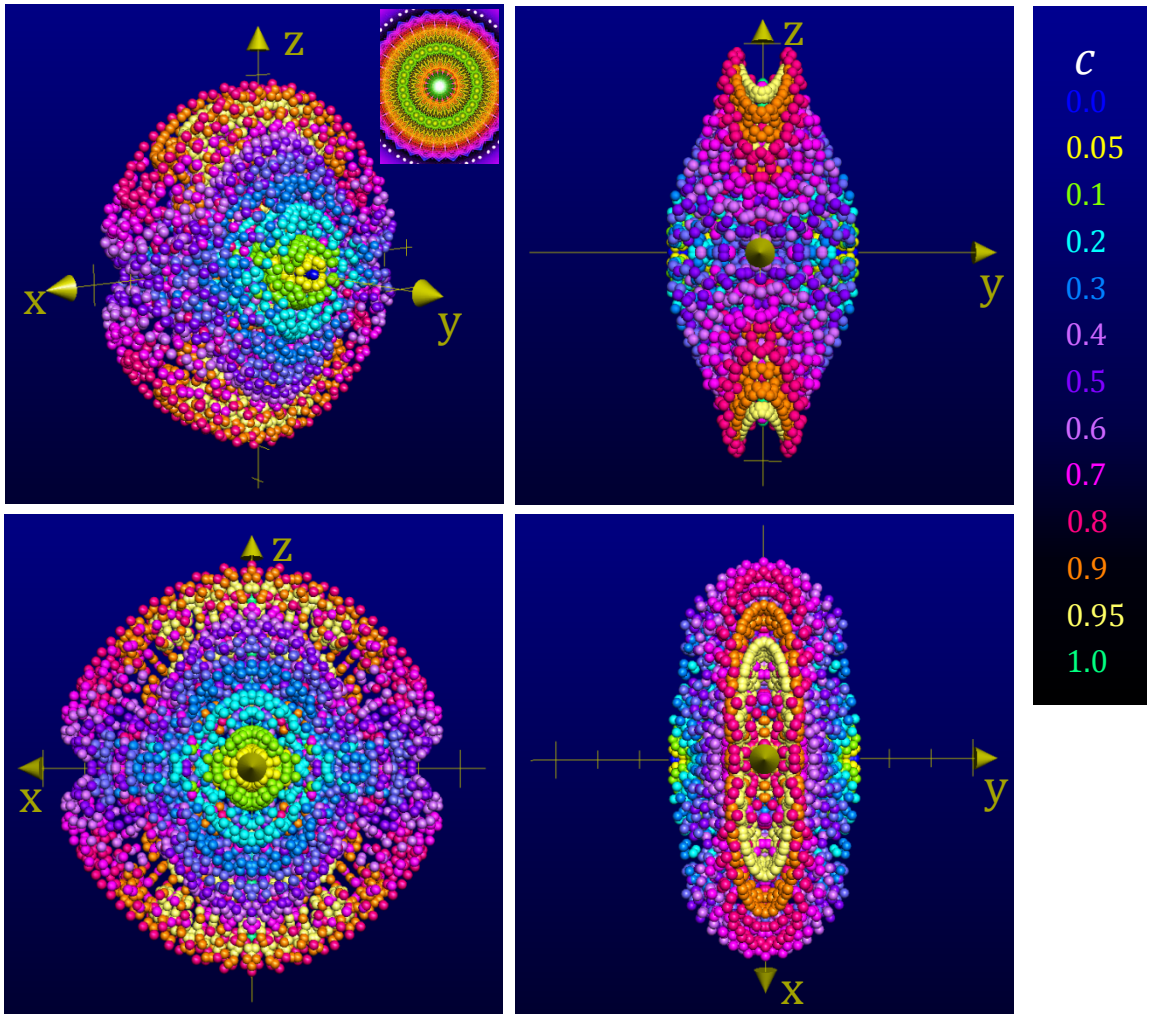

Figure 16. The data in Fig. 15 are presented,
along with other values of the relative dc field amplitude, so that the full range of vorticity control can be appreciated. The maximum torque density amplitude in the *x* direction is roughly equal to that of the *z* direction. Inset is a mandala that seems to capture the appearance of the data. It is of no other importance.

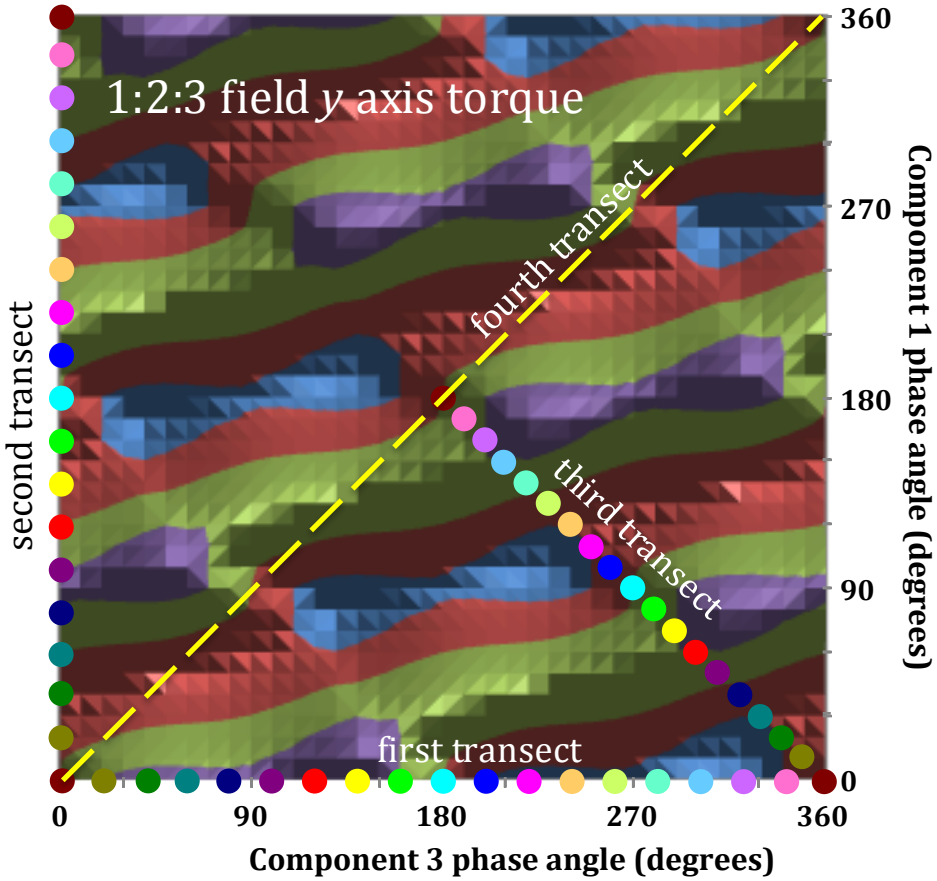

Figure 17. The torque component along y for a 1:2:3 field
is shown along with the color keys for the first, second, and third transects used to generate Fig. 18.

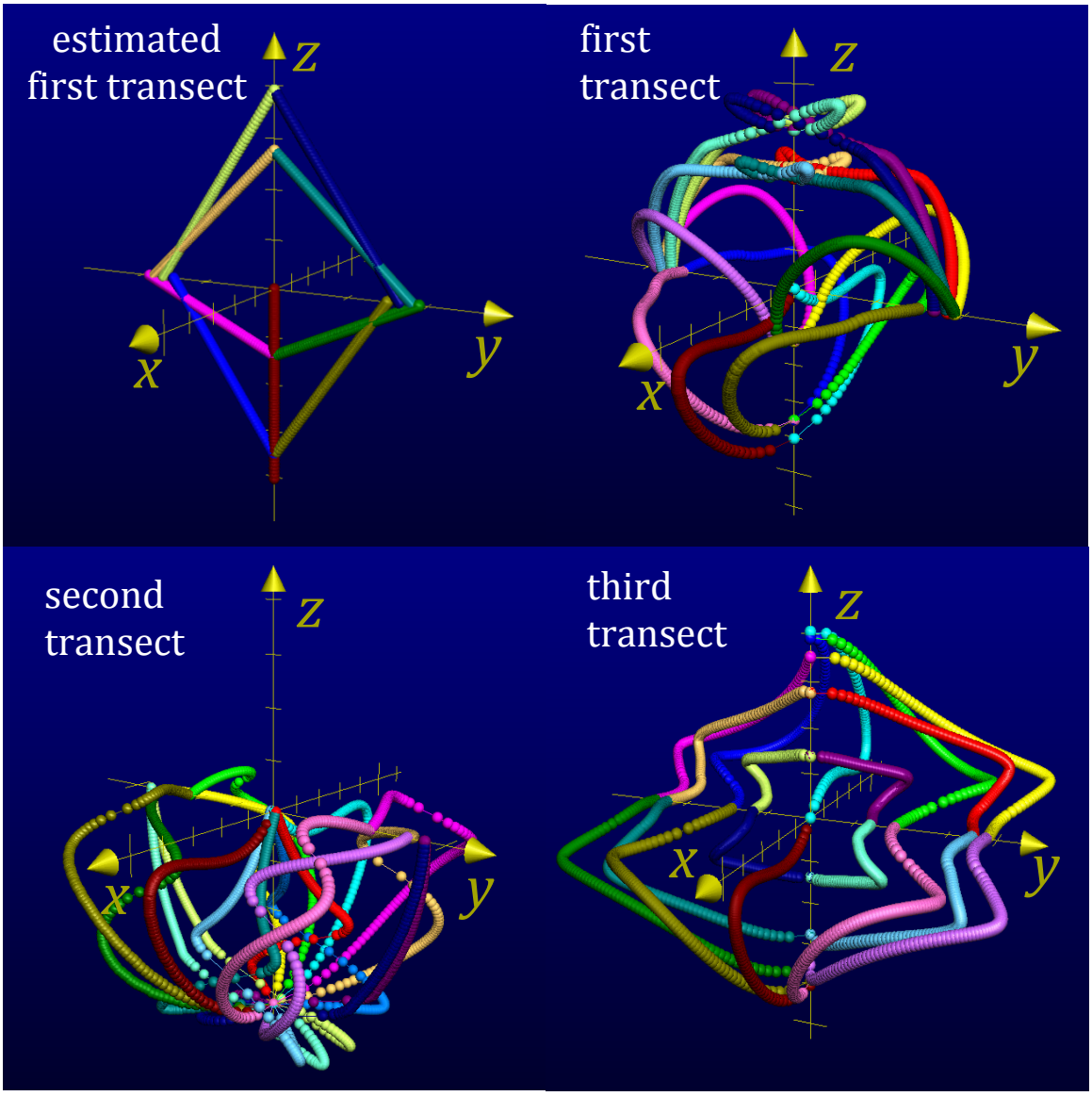

Figure 18. Transects

(top left) The result of using Eq. 3 to estimate the torque density during the transition from 1:2:3 to dc:2:3. Each line represents a different set of phase angles along the first transect shown in Fig. 17. For this transect φ_1=0° and φ_3 increases from 0° to 360° by intervals of 20°. Not all colors in the key are shown because certain phase angles give the same curves. Equivalent φ_3 angles are (90°+n, 90°-n) and (270°+n, 270°-n) where 0°≤n≤90°. Data are for 0≤*c*≤1 in intervals of 0.01. The torques start on the y axis and end on the z axis and are confined to the y-z plane. The tick marks on all axes are separated by 0.025. (top right) When the torque functional in Eq. 2 is used to predict the torque density for points along the first transect the result is dramatically different than the simple rule of mixing. All the colors in the key in Fig. 17 are shown because each point gives a unique curve. These torque curves have substantial deviations from the y-z plane: in some cases the x torque is dominant. If the dc field is reversed (0≥*c*≥-1) both the x and the z components of the torque are reversed. (bottom left & right) Torque functional calculations for points along the second and third transects during the transition from 1:2:3 to dc:2:3. The key for the colors is given in Fig.17. Again, in some cases the *x* torque dominates. If the dc field component is reversed (0≥*c*≥-1) both the *x* and the *z* components of the torque are reversed, which would fill out the upper hemisphere for second transect, but do nothing for the third transect.

6.7 The prediction of vorticity orbits

Heterodyning of the applied 1+dc:2:3 field produces a rich variety of vorticity orbits that are both interesting and potentially useful for a number of applications. We have numerically investigated these orbits for the dc bias c=0.5. In Fig. 19 are shown the simplest possible heterodyne orbits, taken along the four transects shown in Fig. 17. In the laboratory the first transect would be realized by slightly detuning the field frequency along the z axis by Δf. The second transect would be obtained by detuning the frequency of the x component. The third transect requires detuning both of these field components by equal and opposite amounts, and for the fourth transect by equal amounts.

The fourth transect is a bit of a disappointment, as the torque density barely changes, but the other transects produce striking results. The first and second transects produce orbits with a net torque around the z axis (averaged over one orbital cycle) but with zero net torques around the other axes. For these orbits the mixing is persistent. The orbit for the third transect is interesting in that it produces zero net torque around any of the principal axes, which would enable complex mixing in freestanding droplets without incurring any net migration of the droplet. This mixing strategy would be ideal for the development of parallel bioassays of containerless droplet arrays, perhaps comprised of millions of droplets. The fourth transect produces a non-zero net torque around the x axis alone.

The phenomenology of these vorticity orbits is much richer than indicated, Fig. 19 being only the tip of the iceberg. Fig. 20 shows the influence of adding a phase offset to one of the field components, in this case the x component, to create transects that are parallel to those already discussed. The top figure shows a family of orbits obtained by transects parallel to the third transect in Fig. 17. This set of orbits was obtained by adding phases from 0-180° in increments of 10°. The rather confined vorticity orbit in Fig. 19 grows into large orbits and finally collapses back into the tiny fish-shaped orbit at a phase shift of 180°, but reflected in the y-z plane.

The same phase shifts were used to generate a set of orbits for a set of transects parallel to the second transect, generating the set of widely disparate vorticity orbits in the bottom plot of Fig. 19. Adjustment of the relative phase enables a great deal of control over the dynamics of vorticity induced by biased rational triad fields.

Finally, we briefly investigated vorticity orbits for a few cases where the field frequencies, along the x and z axes, are detuned by unequal amounts, specifically by 2:1. These orbits, shown in Fig. 21, are really elaborate. One can only imagine the complexity that would emerge if we applied phase shifts to these transects. But the situation is bad enough already, so we did not pursue this topic further. The question at this point is whether or not these orbits actually exist.

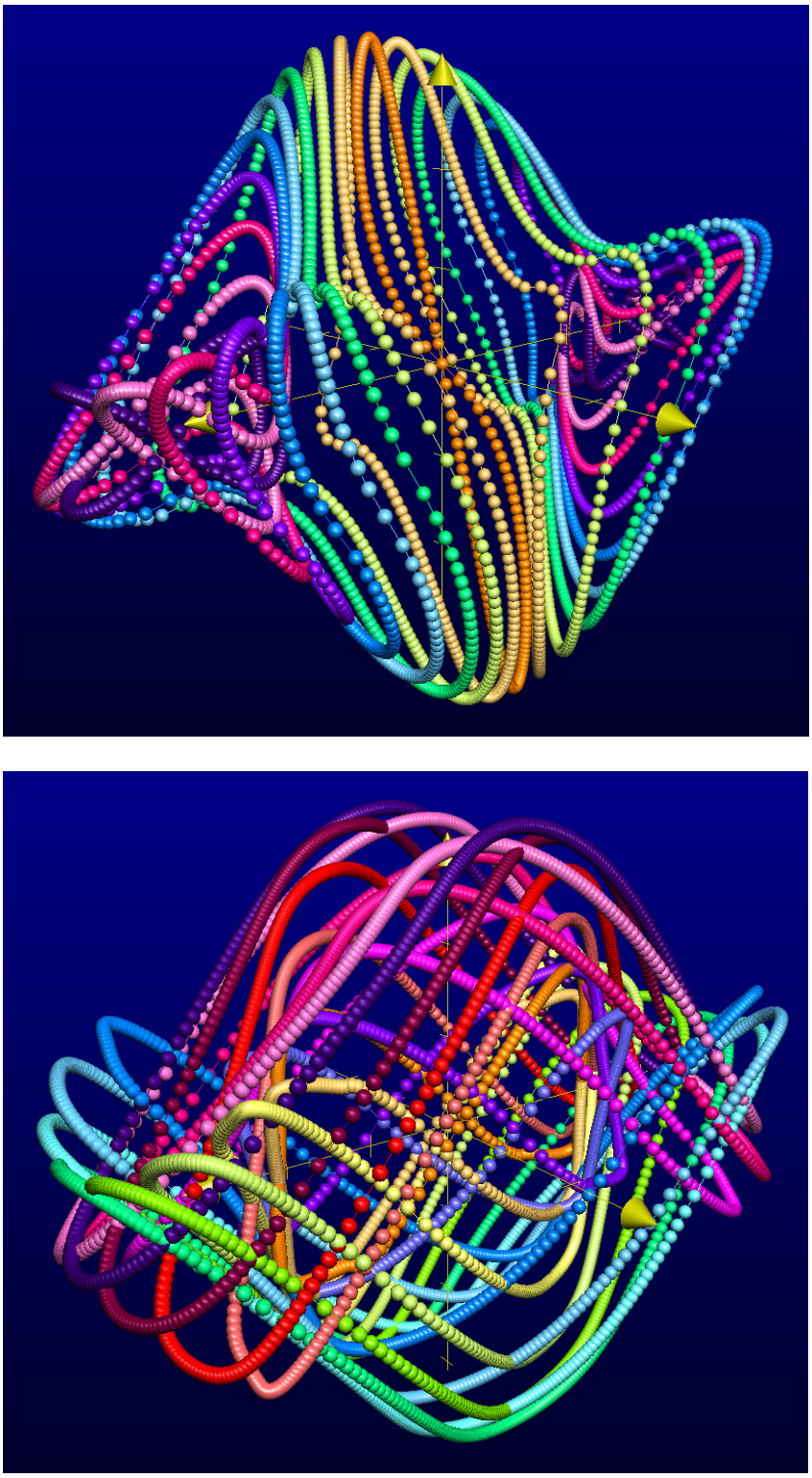

Figure 19. The heterodyne orbits
are sensitive to the relative phase, which provides a simple means of controlling the vorticity orbits.

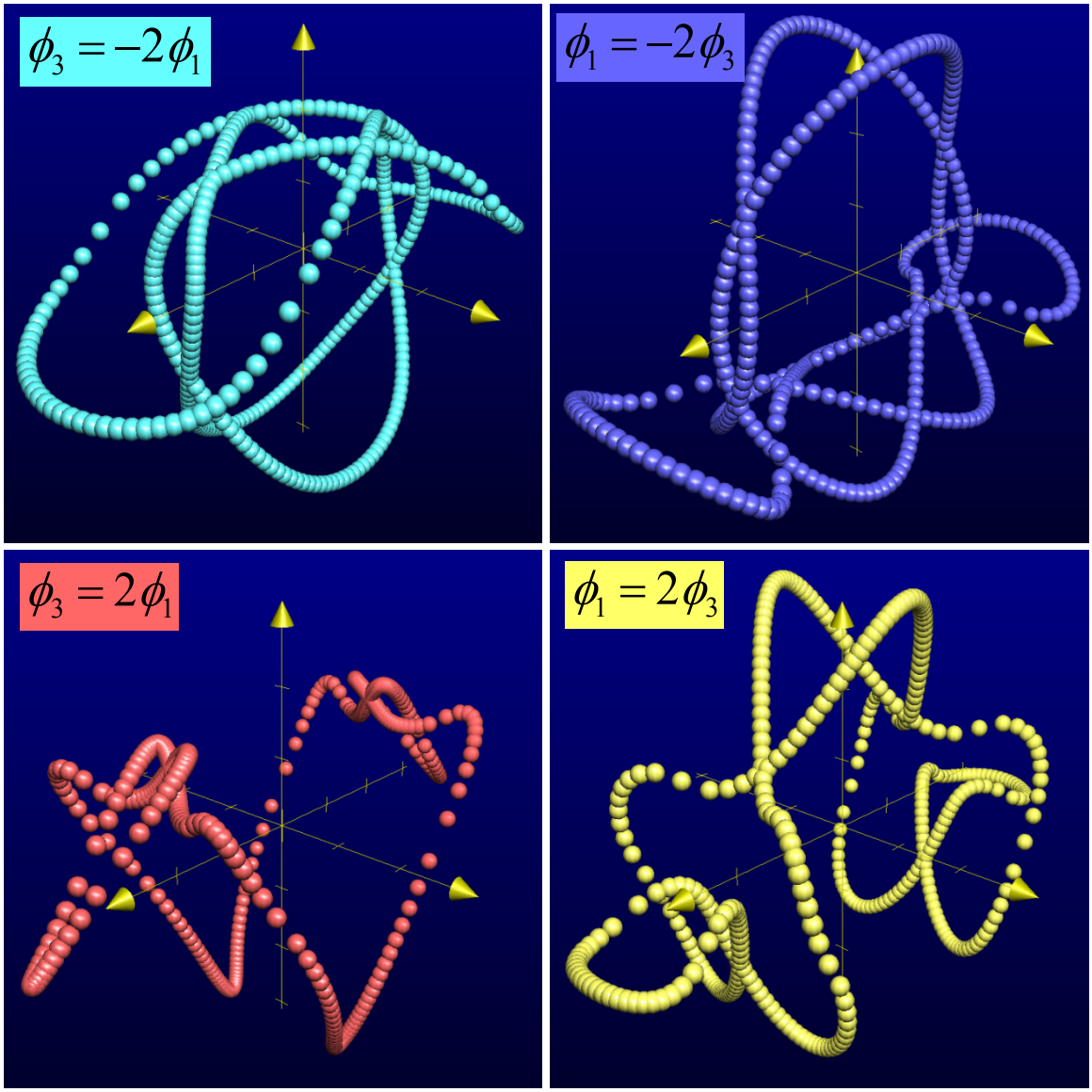

Figure 20. Complex vorticity vector orbits
occur when the field components are detuned by different amounts. Here we consider four simple cases that arise when the *x* and *z* field components are detuned by a ratio of 2:1. Adding a constant phase shift to either field component will alter these orbits. The point is that heterodyning can produce complex variations in the magnitude and direction of the vorticity vector.

6.8 Experimental set up

The magnetic particle suspension consisted of molybdenum-Permalloy platelets ~50 μm across by 0.4 μm thick (Novamet Corp.) dispersed into isopropyl alcohol at a low volume fraction.

For the 1:2:3 rational triad field studied in this work the fundamental frequency was 36 Hz (*f* in Eq. 1) and all three field components were 150 Oe (rms). The spatially uniform triaxial ac magnetic fields were produced by three orthogonally-nested Helmholtz coils. Two of these operated in series resonance with computer-controlled fractal capacitor banks. The third coil was driven directly in voltage mode by a BI-90 operational amplifier. The phase

shift of this coil at its operational frequency of 36 Hz was measured as +68° with a Hewlett-Packard LCR bridge. To compensate for this phase shift we added this phase to the signal output to drive the BI-90.

The signals for the three field components were produced by phase-locked *via* two Agilent/HP function generators (equipped with Option 005), allowing for stable and accurate control of the phase angle of each field component. Note that if these signals are simply produced from separate signal generators there will be a very slow phase modulation between the components due to the finite difference in the oscillator frequency of each function generator. And simply running two separate signal generators off the same oscillator does not control their phase relation. Because all of our measurements are strongly dependent on phase, Option 005 is necessary.

To quantify the magnitude of the vorticity, the torque density of the suspension was computed from measured angular displacements on a custom-built torsion balance. In this case the suspension (1.5 vol%) was contained in a small vial (1.8 mL) attached at the end of the torsion balance and suspended into the central cavity of the Helmholtz coils *via* a 96.0 cm-long, 0.75 mm-diameter nylon fiber with a torsion constant of ~13 □N·m rad^{-1}.

6.9 Results and Discussion

All of the above predictions depend on one key point: the appearance of torque along the *x* axis when a dc field is applied parallel to this axis. Recall that this torque does not exist for *c*=0 or 1, but is only expected for intermediate values, i.e. during the symmetry transition. In fact, upon the application of the dc bias this torque does appear, and is strong, which came as no small relief. Fig. 22 shows the measured torque density along each of the three field components for the the 1+dc:2:3 biased triaxial field with *c*=0.7, where both the ac and dc contributions of the biased field component have equal rms amplitudes. These experimental data were taken for a square lattice of points in the phase angle plane of Fig. 17 on 10° intervals, so in each of these three plots there are 36x36=1296 data points. However, the symmetry of the data reduces the required number of measurements for each plot to a fourth of this, 324.

The set of measured vorticity vectors is plotted in Fig. 23 (top). These data can be compared to the computed data for the corresponding value of *c*=0.7 in Fig. 15. The detailed appearance is different, but the essential point is that the locus of points does not simply lie in the *y*-*z* plane, but has significant components along the *x* axis. In fact, the maximum specific torque density (torque density divided by the volume fraction of particles) along the *x* axis is 476 J/m^3, which can be compared to the maxima of 1127 and 993 J/m^3 along the *y* and *z* axes, respectively. Heterodyning can be expected to create three-dimensional orbits that intersect these points.

The progression of the measured torque density as the dc field is increased from *c*=0 to 1 is shown in Fig. 23 (bottom) for points taken along the third transect of Fig. 17, but with a phase offset of +60° applied to the *x* axis (36 Hz) component, to ensure a significant torque density around this axis [see Fig. 22 (top)]. These curves start on the *y* axis and terminate on the *z* axis and although they differ from the computed curves for the third transect, Fig. 18 (bottom right), they do share the characteristic of being symmetric under a 180° rotation around the *y* axis. Again, the essential point is that these curves are substantially different than the reasonable prediction given in Eq. 3 in that they are not confined to the *y*-*z* plane.

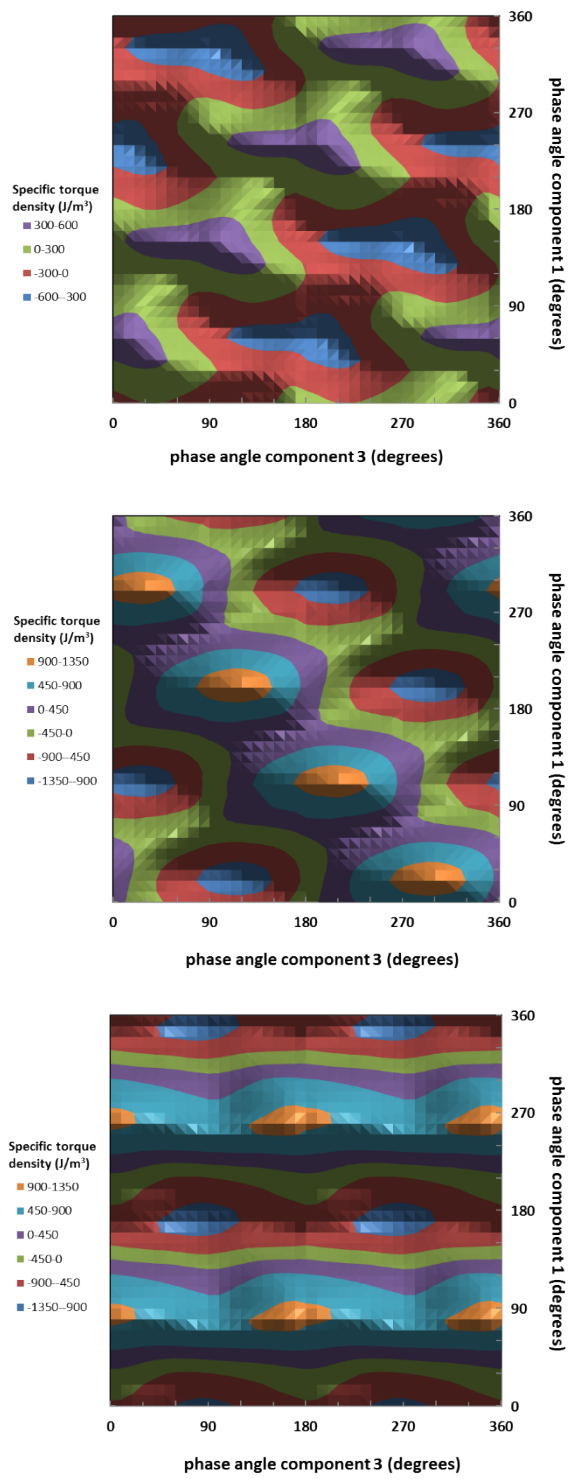

Figure 21. Experimental torque density plots
for the x (top), y (middle) and z (bottom) torque components. These data are for the 1:2:3 field with *c*=0.7.

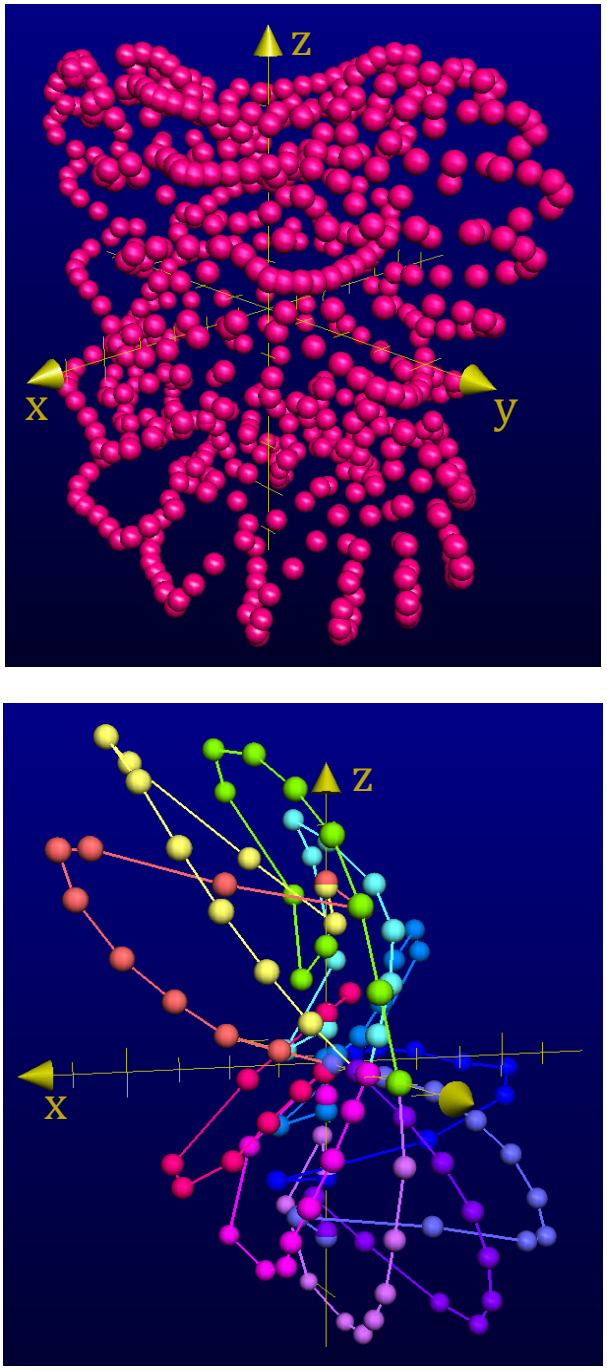

Figure 22. (top) **The locus of possible vorticity vectors** for the 1+dc:2:3 biased rational triad with *c*=0.7. These points span all three spatial dimensions, indicating that complex vorticity orbits can exist. (bottom) The evolution of the vorticity vectors taken along the third transect as *c* is increased from 0 to 1. Each colored curve is for a different set of phase angles. Each curve starts on the *y* axis and terminates on the *z* axis. The important feature is the large torque density amplitude along the *x* axis.

The vorticity orbits can be obtained by detuning one or more field components. To be clear about the experimental parameters the field can be written

$$H_0^{-1}\mathbf{H}_0(t) = \sin(s + 2\pi\Delta f_1 t + \phi_1)\hat{\mathbf{x}} + \sin(2s)\hat{\mathbf{y}} + \frac{1}{\sqrt{2}}\left[\sin(3s + 2\pi\Delta f_3 t) + \frac{1}{\sqrt{2}}\right]\hat{\mathbf{z}}$$

where $s=ft$ is the reduced time. We have included the parameters Δf_1 and Δf_2 to indicate detuning of the first and third field field components. The principal vorticity orbits for the 1+dc:2:3 field, in Fig. 24, are for zero offset phase, i.e. $\phi_1 = 0$, and correspond to the four transects in Fig. 17, which are

$$\Delta f_1 = 0,\ \Delta f_3 = const;\ \Delta f_1 = const,\ \Delta f_3 = 0;\ \Delta f_3 = -\Delta f_1;\ \text{and}\ \Delta f_3 = \Delta f_1$$

respectively. In Fig. 25 are shown the families of orbits that emerge when the offset phase is increased from 0 to 340° by 20° intervals. Note that many of the points are the same in these plots (since they must be comprised of the available data points in Fig. 23), but the orbits interconnect these points in different ways.

The complexity of these orbits can be appreciated by one single phase modulation example, wherein we monitored the x component of the torque for the frequencies 36.1, 72 and 108.2 Hz and recorded the torque density as a funciton of time. This direction observation of this one component of the vorticity orbit is plotted in Fig. 26 (top), which shows a periodic behavior that is not a simple sinusoid. The phase plot in Fig. 26 (bottom) shows strongly non-harmonic dynamics. For this particular circumstance the variations in the torque density are symmetric about zero, indicating zero time-averaged vorticity, but there are many phase modulation cases where the vorticity never changes sign.

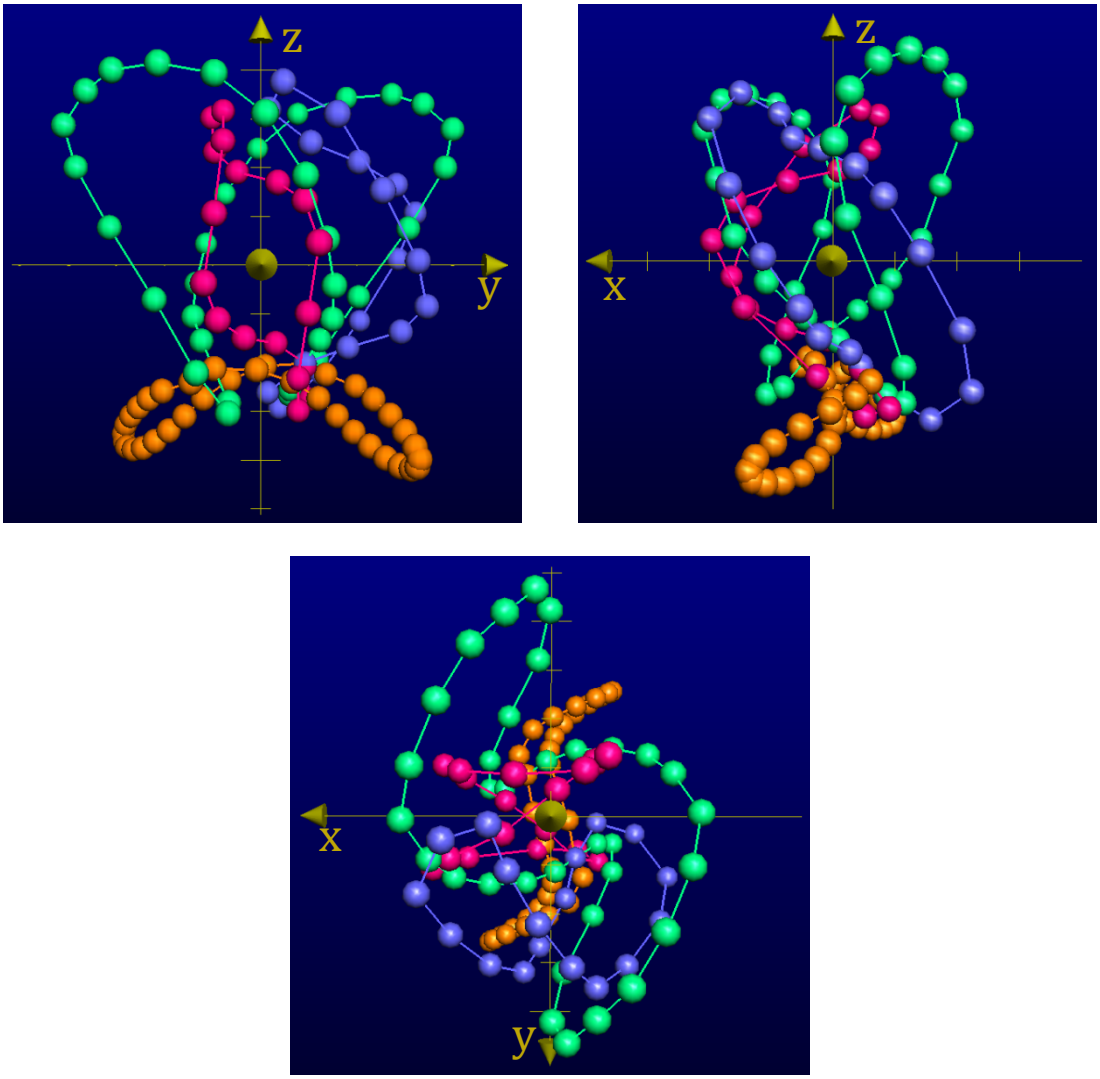

Figure 23. Experimental vorticity orbits along the four transects shown in Fig. 17 are viewed along each field component. Transect one is depicted in orange, transect two in green, transect three in violet, transect four in red. When averaged over a cycle, transects one and two have a net *z* axis vorticity, transect four has a net *x* axis vorticity, and transect three has a net *y* axis vorticity, in concurrence with the predictions from the torque density functional in Fig. 19.

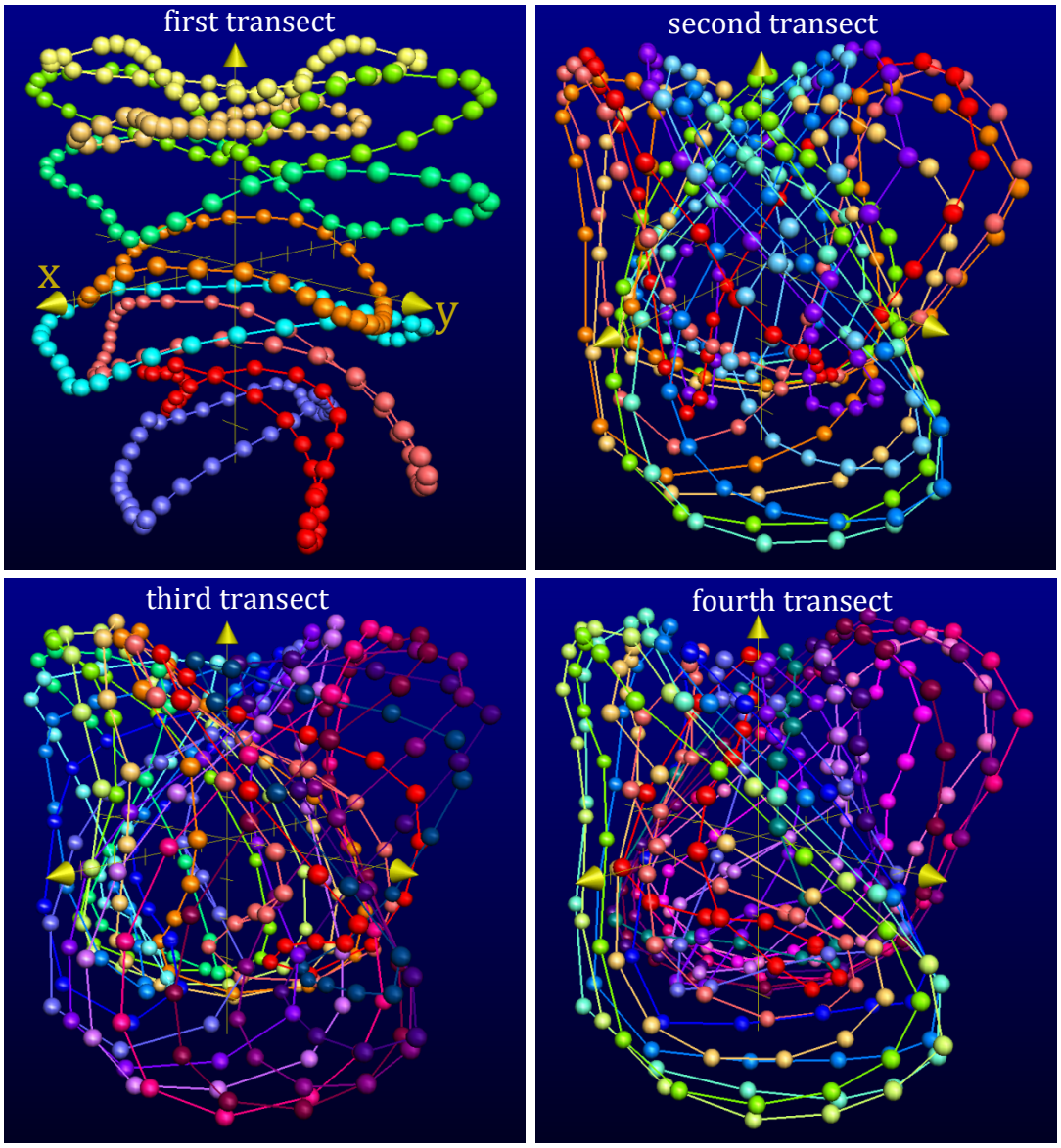

Figure 24. Phase offsets significantly alter the vorticity orbits
for each of the four transects shown in Fig. 24. For each transect curves are presented for successive parallel transects at 20° intervals.

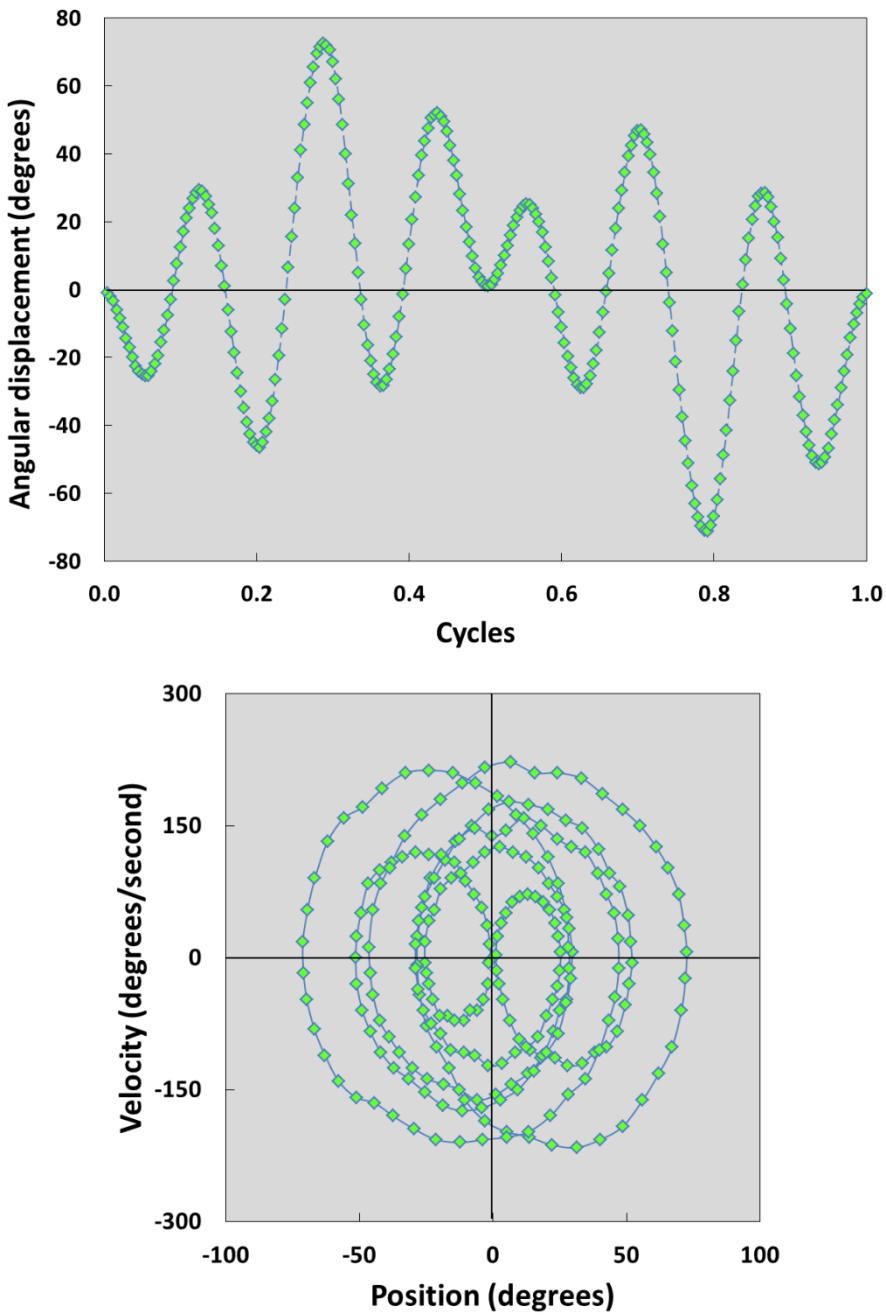

Figure 25. For the phase modulated 1+dc:2:3 with *c*=0.7,
given by the frequencies 36.1, 72 and 108.2 Hz the *x* axis torque is plotted as a function of cycles (top) and versus the time derivative of the torque (bottom) to make a phase plot. The torque is periodic, though not a simple sinusoid, and the phase plot indicates a strongly non-harmonic dynamics (bottom). For a harmonic oscillator this phase plot would be an ellipsoid.

7. CONCLUSIONS

We have shown that applying a dc field parallel to a carefully chosen alternating component of an ac/ac/ac rational triad field can create a transition in the field symmetry. By exploiting this transition we have shown through theory and experiment that we can point the vorticity vector in a wide range of directions comprising the full three spatial dimensions. The direction of the vorticity vector can be controlled by the relative phases between field components and the magnetude of the dc field. Detuning one or more field components to create phase modulation causes the vorticity vector to trace out complex orbits of a wide variety, creating very roust multiaxial stirring. This multiaxial, noncontact stirring is attractive for applications where the fluid volume has complex boundaries, or is congested. Multiaxial stirring would be an effective way to deal with the dead zones that can occur when stirring around a single axis and could eliminate the accumulation of particulates that frequently occurs in such mixing. But beyond the practical implications of this new technology there is a lot of interesting science. A principal remaining challenge is a first-principles, microscopic theory of the dynamics of particles in these fields that would enable more accurate predictions of the vorticity orbits and the other phenomena we have observed.

8. REFERENCES

1. S. Chandrasekhar, Hydrodynamic and Hydromagnetic Stability (Dover, New York, 1981), pp. 9–71.
2. A.V. Getling, Rayleigh-Bénard Convection: Structures and Dynamics (World Scientific, Singapore, 1997).
3. Dynamics of Spatio-Temporal Cellular Structures: Henri Bénard Centenary Review, edited by I. Mutabazi, J. E. Wesfreid, and E. Guyon (Springer, Berlin, 2005).
4. D.P. Lalas and S. Carmi, *Phys. Fluids*, 1971, **14**, 436.
5. R.A. Curtis, *Phys. Fluids*, 1971, **14**, 2096.
6. K.J. Solis and J.E. Martin, Isothermal magnetic advection: creating functional fluid flows for heat and mass transfer, *Appl. Phys. Lett.*, 2010, **97**, 034101.
7. J.E. Martin and K.J. Solis, Symmetry-breaking magnetic fields create a vortex fluid that exhibits a negative viscosity, active wetting, and strong mixing, *Soft Matter*, 2014, **10**, 3993–4002.
8. K.J. Solis and J.E. Martin, Torque density measurements on vortex fluids produced by symmetry-breaking rational magnetic fields, *Soft Matter*, 2014, **10**, 6139–6146.
9. K.J. Solis and J.E. Martin, Complex magnetic fields breathe life into fluids, *Soft Matter*, 2014, **10**, 9136–9142.
10. K.J. Solis and J.E. Martin, Multiaxial fields drive the thermal conductivity switching of a magneto-responsive platelet suspension, *Soft Matter*, 2013, **9**, 9182–9188.
11. J.E. Martin and K.J. Solis, Fully alternating, triaxial electric or magnetic fields offer new routes to fluid vorticity, *Soft Matter*, 2015, **11**, 241–254.
12. J.E. Martin, Theory of strong intrinsic mixing of particle suspensions in vortex magnetic fields, *Phys. Rev. E: Stat., Nonlinear, Soft Matter Phys.*, 2009, **79**, 011503.
13. J.E. Martin, A resonant biaxial Helmholtz coil employing a fractal capacitor bank, *Rev. Sci. Instrum.*, 2013, **84**, 094704.
14. J.E. Martin, R.A. Anderson, and C.P. Tigges, Simulation of the athermal coarsening of composites structured by a biaxial field, *J. Chem. Phys.*, 1998, 108, 7887.
15. J.E. Martin, E. Venturini, J. Odinek, and R.A. Anderson, Anisotropic magnetism in field-structured composites, *Phys. Rev. E*, 2000, **61**, 2818–2830.

16. J.E. Martin, R.A. Anderson, and R.L. Williamson, Generating strange magnetic and dielectric interactions: Classical molecules and particle foams, *J. Chem. Phys.*, 2003, **118**, 1557–1570.

17. B. Schwarzchild, Physics Nobel Prize Goes to Tsui, Stormer and Laughlin for the Fractional Quantum Hall Effect, *Physics Today*, December 1998.

9. DISTRIBUTION

4 Lawrence Livermore National Laboratory
Attn: N. Dunipace (1)
P.O. Box 808, MS L-795
Livermore, CA 94551-0808

1	MS0899	Technical Library	9536 (electronic copy)
1	MS0359	D. Chavez, LDRD Office	1911
1	MS0115	OFA/NFE Agreements	10012
1	MS0161	Legal Technology Transfer Center	11500

Sandia National Laboratories